Diplomarbeit

zum Erwerb des akademischen Grades eines Diplomingenieurs
der Angewandten Geowissenschaften und Geophysik

eingereicht am

Department Angewandte Geowissenschaften und Geophysik
Lehrstuhl für Geophysik

von

Christina Schell

betreut von

Ao.Univ.-Prof.Dr.phil. Robert Scholger
Department Angewandte Geowissenschaften und Geophysik
Lehrstuhl für Geophysik
Montanuniversität Leoben

Dr. Norbert Schleifer
Wintershall AG Germany

Leoben, Dezember 2006

Danksagung

Ich möchte mich bei Herrn ao.Univ.-Prof.Dr.phil. Robert Scholger für die kompetente Betreuung, die hilfreichen Tipps und die freundliche Unterstützung während dieser Diplomarbeit bedanken.

Bedanken möchte ich mich auch bei Dr. Norbert Schleifer, der mit mir diese Arbeit begonnen hat und mir bei den petrophysikalischen Messungen hilfreich zur Seite stand.

Für die Finanzierung dieser Diplomarbeit möchte ich mich bei der Österreichischen Akademie der Wissenschaften bedanken.

Weiters möchte ich mich beim Landesmuseum Joanneum Graz für die Bereitstellung des Probenmaterials aus Bad Gleichenberg bedanken.

Dem Department für Angewandte Geowissenschaften und Geophysik, Lehrstuhl für Geophysik, danke ich für den Arbeitsplatz und die Möglichkeit zur Durchführung der petrophysikalischen Messungen im hauseigenen Labor.

Meinen Eltern danke ich für ihre bedingungslose Unterstützung während meines Studiums, ihre Zuversicht und den Glauben an mich, denn ohne sie wäre ich wohl nie soweit gekommen.

Ich versichere eidesstattlich,
die vorliegende Arbeit selbständig
unter Verwendung der angegebenen Literatur
verfasst zu haben.

Christina Schell

Leoben, Dezember 2006

Characterization of geological structures by using petrophysical parameters and the effect of anisotropy

Diploma Thesis

Christina Schell

Contents

Abstract

The interpretation of petrophysical data sets is a common tool for the identification of different lithologies as the variation of mineralogy, texture and porosity is accompanied by varying physical properties. A special issue is the analysis of the directional dependence of the petrophysical properties assumed to yield to a further characterization of the lithologies and the relation to the geological origin. Three different geological structures, the shield volcano of Bad Gleichenberg, Austria, locations within the Bohemian Massif, Austria, and the Bosumtwi impact structure in Ghana, Africa, were observed in terms of their petrophysical properties (electrical, elastic and magnetic), the anisotropy coefficient and the history of origins. The results of the study allow a characterization of the various lithologies involved in terms of petrophysical properties whereas the analysis of the coefficient of anisotropy not always succeeds. In case of Bad Gleichenberg a differentiation between the various layers of the shield volcano is obvious. The analysis of the coefficient of anisotropy is difficult. The locations investigated within the Bohemian Massif show a dependence of physical properties and anisotropy associated with the distance to the fault system. The drill cores of the Bosumtwi impact crater show a differentation of various layers within the structure in petrophysical parameters and the coefficient of anisotropy.

Zusammenfassung

Die Untersuchung petrophysikalischer Parameter zur Beschreibung von Gesteinstypen wird oftmals verwendet, da die physikalischen Parameter Veränderungen in der Mineralogie, Struktur und auch Porosität erkennen lassen. Die Beobachtung der Richtungsabhängigkeit der Eigenschaften ist eine Erweiterung der Untersuchung und soll zusätzliche Informationen über das Gestein und dessen Herkunft liefern. Drei geologische Strukturen wurden im Hinblick auf ihre petrophysikalischen Eigenschaften (elektrische, elastische und magnetische), den Anisotropiekoeffizient und den Zusammenhang mit der Entstehungsgeschichte untersucht. Im ersten Fall konnten die Gesteinstypen und der Schichtaufbau des Schildvulkans von Bad Gleichenberg, Österreich, mit Hilfe eines Bohrkernes charakterisiert werden. Da die Formation relativ ungestört ist, ist die Untersuchung des Anisotropiegrades schwierig. Als zweites wurden Probestellen in der Böhmischen Masse untersucht, die eine Abhängigkeit der petrophysikalischen Eigenschaften mit der Enfernung zur Pfahl Störung zeigen. Zuletzt wurden zwei Bohrkerne aus dem Impaktkrater von Bosumtwi in Ghana, Afrika, untersucht. Die petrophysikalischen Parameter und der Anisotropiekoeffizient erlauben eine Zonierung des Untergrundes. Die vorliegende Untersuchung zeigt, dass die Analyse petrophysikalischer Daten eine Klassifizierung der Gesteine erlaubt. Hinsichtlich des Anisotropiekoeffizienten sind nicht immer aussagekräftige Ergebnisse gefunden worden.

Chapter 1

Introduction

Petrophysical parameters are used to describe physical properties of rocks, e.g. density, porosity, ultrasonic velocity, susceptibility and the anisotropy of magnetic susceptibility (AMS). These features analyzed and considered in comparison to each other allow a distinction of various types of rocks (e.g. Jäger, 2004). Hence, these parameters are used to describe the structure of geological formations (e.g. Kukkonen et. al., 2003; Scholger & Mauritsch, 1992) as well as the influence of cooling or post–cooling processes on the petrophysical characteristics (Sruoga et. al., 2004). Vanorio et. al. (2002) investigated the influence of microtextures on the petrophysical parameters of volcanic rocks. In order to compare petrophysical properties of surveyed rocks with new investigation areas data–acquisition projects are installed (e.g. Lenz et. al., 1996). Thus, the study of petrophysical parameters covers a broad range of applications.

A special challenge is the examination of the petrophysical parameters considering the directional dependence, i.e. anisotropy, in order to give a more detailed information concerning hydrothermal activity, primary flow directions of lava sheets, tectonic overprints and the evolutionary history (Tarling & Hrouda, 1993; Zechner, 2002). Anisotropy occurs as rocks are in general inhomogeneous and consist of structured systems of different mineral components with varying physical properties, shapes, sizes and complicated boundary effects and interactions (Schön, 2004). Moreover, anisotropic features are strongly correlated to structural–textural properties as e.g. layering, orientation of cracks, grain and mineral anisotropy originated by the depositional environment and can therefore be seen as the consequence of the rock forming process or the past rock forming process e.g. metamorphism, orogeny or impact events (Schön, 2004).

The investigation of petrophysical parameters in terms of anisotropy is mainly applied for elastic, electrical and magnetic properties. For the characterization of frac-

tured systems and thus for petroleum reservoirs and hydrogeolgical studies the elastic and electrical properties are the most interesting. In case of the magnetic properties the analysis of the anisotropy of the magnetic susceptibility (AMS) is a well known tool. The interest in studying anisotropic features applying the AMS method to characterize forming processes started with the 1980s (Chadima et. al., 2006). Previous studies in this field of interest reasoned that the investigation of petrophysical data in view of anisotropy yield further information on the forming process of various geological bodies like accretionary wedges (Chadima et. al., 2006) and underplating processes (e.g. Housen & Kanamatsu, 2003). Furthermore the consequence of deformation on minerals was investigated in order to state, which deformation process occurred in the source rock (e.g. Pars & van der Plujm, 2002). Hence anisotropy becomes more and more important in characterization of deformation processes. An enhancement in studying anisotropic features is the investigation whether different lithologies can be distinguished by means of their specific anisotropy.

The survey at hand examines the structure of three different geological situations. The sample locations are different in the evolutionary history and therefore, it is assumed that the petrophysical parameters vary, in particular the anisotropic features. An interpretation of the rock types, the petrophysical properties, the anisotropic features and the geological formation process should allow a significant characterization of the investigated structures.

Firstly, a drill core sinked into the shield volcano of Bad Gleichenberg in Styria/ Austria is investigated, provided by the Landesmuseum Joanneum Graz. The core was drilled in 1981 in the course of a project to identify a thermal water resource (Belocky et. al., 1996). The drill core was investigated by means of a macroscopic description of the lithologies, mineralogical and geochemical measurements allowing a characterization and dating of the volcanic rocks, and an analysis of the rock sequence (Belocky et. al., 1996). Moreover, the susceptibility values along significant lithology changes were observed (Belocky et. al., 1996). The shield volcano was the issue of several previous investigations characterizing the Miocene volcanic activity (e.g. Ebner & Sachsenhofer, 1991), the Miocene volcanic tuff formations (e.g. Ebner, 1981) or the potential of the volcanic rocks as raw material resources (e.g. Ebner, 1990). All investigations dealt in general with the geological and mineralogical features of the area. Within this study, the petrophysical properties electrical resistivity, porosity, bulk density, compressional velocity, susceptibility and AMS measurements are surveyed to obtain further characteristics of the volcanic rock types available and a correlation with

the existing core description. A special issue within the study is the investigation of the directional dependence of the petrophysical properties in order to obtain further information in view of the lithologies involved and the forming process.

Secondly, sample sites located within the South Bohemian Pluton in Upper Austria/Austria are analyzed. The samples were collected in the course of a scientific project funded by the Austrian Science Fund (FWF) in the 1990s. In the course of the project a large number of locations was analyzed in view of paleomagnetic features (e.g. Mauritsch & Reisinger, 1990). Furthermore, the area was investigated in terms of tectonic and kinematic structures (e.g. Wallbrecher et. al., 1990) or isotope ratio investigations for dating purpose (e.g. Frank et. al., 1990). The study at hand examines three sample locations of Schlägel granite in view of the change in petrophysical properties in order to characterize the influence due to the formation of the Bavarian Pfahl on the rock physics. The investigation should yield to a differentiation of the sample locations as the deformation and hence, the coefficient of anisotropy, should decrease with increasing distance to the Bavarian Pfahl.

Finally, the Bosumtwi Meteorite Impact Structure in Ghana/Africa formed by a meteorite impact about 1.07 Ma ago (Koeberl et. al, 1998) is examined. In 2004, a deep drilling project of the International Scientific Drilling Program (ICDP) was realized where two cores, LB-07A and LB-08A, were drilled. The cores should lead to more detailed information on the internal structure of the crater and the various lithologies involved. Analyzing the samples in terms of anisotropy the meteorite impact event is assumed to deliver a specific anisotropy for each lithology involved and therefore a characterization of different layers and their boundaries should be possible. In order to survey these aspects especially the AMS measurement is used as previous studies have already shown good results in applying this method (e.g. Scholger and Mauritsch, 1992).

The overall goal to reach is the characterization of the investigated lithologies using petrophysical properties and their anisotropic features. In addition the geological structure and the history of origin is examined and correlated with the petrophysical results yielding to a detailed description of the structure in geological and geophysical view.

Chapter 2

Basic Theory and Methods

2.1 Density and Porosity

2.1.1 Basic principles of density

Density is a physical property which is dependent on mineralogy and porosity. Due to varieties in theses two features among various rock types density changes significantly (Olhoeft and Johnson, 1989). The definition of density d is given by the quotient of mass m and volume V of a specific material with the SI unit $kg\ m^{-3}$ (Schön, 2004).

$$d = \frac{m}{V} \qquad \left[kg\ m^{-3}\right]$$

As a result of heterogeneity predominant in rocks diverse kinds of density have to be distinguished. The various densities are related to distinct parts or components contained in the material mixture we call "rocks". Hence, the bulk density d which is the mean density of the considered rocks including pores , e.g. density of sandstone, the density of an individual rock component i d_i, e.g. density of quartz, the mean density of the solid matrix material d_m, e.g. density of a carbonate matrix excluding pores and the mean density of the pore or fracture fluid d_p, e.g. density of pore water, can be differentiated (Schön, 2004).

On the basis of these principles the density of rocks is dependent on the mineral content, the content of enclosed pore or fracture space and the filling material. Thus, rock types have to be distinguished due to their origin. The volume content of pores and cracks is relatively small in igneous rocks and in most metamorphic rocks and therefore the influence can be denied. However, in sedimentary rocks the influence of pore volume (porosity) and pore filling is generally strong (Schön, 2004).

2.1.2 Basic principles of porosity

Porosity is a dimensionless quantity mostly expressed in terms of percentage describing the part of the total volume of a rock which is not occupied by solid components (figure 2.1).

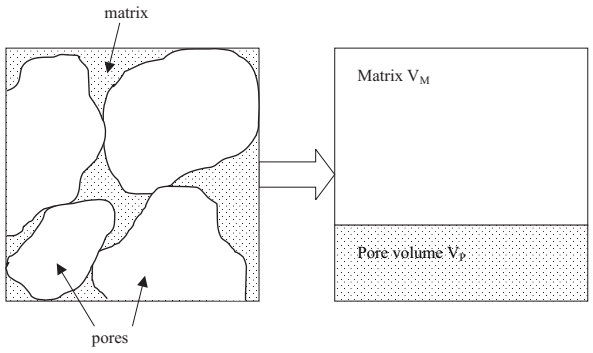

Figure 2.1: Definition of porosity (Schön, 2004)

Therefore pores are local enlargements in a rock providing most of the volume available for fluid storage. The pore space is connected via pore throats who restrict the fluid flow. Porosity ϕ is defined by the ratio of the pore volume V_P to the total volume V_T of a sample (Schön, 2004).

$$\phi = \frac{V_P}{V_T} \cdot 100 \qquad [\%]$$

As porosity is the result of various geological, physical and chemical processes it is a complex task and different kinds of porosity are known and have to be distinguished. Hence, two main types of porosity can be differentiated, "primary porosity", generated during the genesis of the rock, and "secondary porosity", a variation of the primary porosity due to tectonic and chemical processes or dissolution (Schön, 2004).

Another problem is the intricate geometry of pore space in classifying the type and degree of interconnection between the pores as the pores can be interconnected or partially isolated from each other (e.g. enclosed by solid matrix). Thus, the porosity is an individual value for each rock and in general difficult to give. An approximation on porosity for different rocks can only be given in terms of comparison. Thus, high porous marine sediments and unconsolidated sediments have a higher porosity than igneous and most metamorphic rock types. The influence of fractures can change the value for porosity significantly and has therefore to be considered independently (Schön, 2004).

2.1.3 Method of laboratory measurement

The determination of density and porosity is done by using the Buoyancy Method based on the Archimedes‘ principle as this method allows to observe bulk density, apparent grain density and apparent porosity. Further on calculations on the total volume, the pore volume and the matrix volume are carried out. In order to get the parameters stated above the samples are weighed in dry, saturated and saturated condition under buoyancy.

Therefore the samples are dried in a heater at $\sim 80°C$ for two days before weighing in oven dry condition. Afterwards they are going to be saturated with a 0.058 $\%weight$ NaCl solution. The saturation of the samples is achieved in a vacuum environment at ~ -0.85bar which is generated in a vacuum stable tank (figure 2.2. On top of the bowl is a recloseable funnel located which allows the saturation of the samples while being in vacuum. To be certain that a complete saturation of the samples is achieved they are kept in vacuum for 12 hours and are evacuated another time after this period. Hence, an entire saturation is assumed.

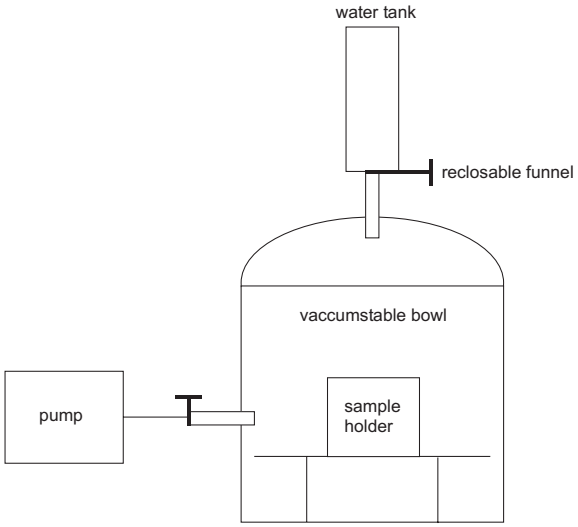

Figure 2.2: Principle sketch of the saturation operation

Following this the specimen are weighed in saturated condition after removing the surface water. Subsequently the samples are weighed under buoyancy in a bath of 0.058 $\%weight$ NaCl solution, the same fluid used in the saturation process. For the weighing purpose a Sartorius laboratory scales, Laboratory LC 6200 S, with an error bar of $\pm$ 0.01g is used.

In order to eliminate weighing errors all measurements are repeated three times.

Finally the parameters named earlier are calculated using the listed formulae (Olhoeft and Johnson, 1989) with the paramaters W_d the weight in dry condition in g, W_s the weight of the saturated sample in g, W_b the weight of the saturated sample under buoyancy in g and d_W the density of water at 20°C ($0,998\ gcm^{-3}$):

Total Volume	$V_T = V_P + V_M$	$\left[cm^3\right]$
Pore Volume	$V_P = \frac{W_s - W_d}{d_W}$	$\left[cm^3\right]$
Matrix Volume	$V_M = \frac{W_d - W_b}{d_W}$	$\left[cm^3\right]$
Porosity	$\phi = \left[\frac{W_s - W_d}{V_T * d_W}\right] * 100$	[%]
Bulk Density	$d = \frac{W_d}{(W_s - W_b) * d_W}$	$\left[gcm^{-3}\right]$
Grain Density	$d_g = \frac{W_d}{(W_d - W_b) * d_W}$	$\left[gcm^{-3}\right]$

2.2 Elastic Properties

2.2.1 Basic principles of elastic properties

The description of elastic wave propagation in rocks is based on the theory of elasticity. The wave propagation is dependent on the elastic properties of the rock forming minerals, their fractional volume, the pore filling, the grain contact, cementation or bonding properties, pressure and temperature. The range of velocities within a group of rocks varies due to variations of the parameters stated above (Schön, 2004).

Although the determination of elastic properties for various types of rocks is difficult a few coherences can be summarized. Generally an increase of density results in an increase of velocity. Therefore it can be stated that acidic constituents e. g. quartz have lower densities and show lower velocities than basic minerals e. g. olivine. Another observation is the decrease in velocity due to an increase of porosity and fracturing, but an increase in velocity occurs with an increase of fluid saturation (water, brine, oil) (Schön, 2004).

Velocity measurements along orthogonal sample axis can also be used to determine effects of anisotropy as for example the non-uniform application of external forces

results in directional variations of the elastic properties and the velocity of elastic waves (Schön, 2004). Five possible sources of seismic anisotropy are listed by Crampin and Lovell (1991):

- aligned crystals
- direct stress-induced anisotropy
- lithologic anisotropy (aligned grains)
- structural anisotropy (fine layering)
- stress aligned crack-induced anisotropy

A complete characterization of the elastic anisotropy of a sample requires measurements on more than two perpendicular directions, but a simplified description can be done by using the maximum and minimum measured values ($v_{\max}, v_{\min}$) or the values measured parallel and perpendicular to the stratification, foliation or main crack orientation ($v_{\shortparallel}, v_{\perp}$). By using one of these pairs of values the anisotropy coefficient A_v and the anisotropy ratio A_v^* can be calculated (Schön, 2004).

$$A_v = \frac{v_{\max} - v_{\min}}{v_{\min}}$$

$$A_v^* = \frac{v_{\max}}{v_{\min}} = A_v + 1$$

Applying this formulae two significant tendencies in rocks can be specified. Firstly, it can be stated that among magmatic and metamorphic rocks gneiss and schist have the highest values of anisotropy. Secondly, the anisotropy for sedimentary rocks increases from sandstone to siltstone and shale (Schön, 2004).

2.2.2 Method of laboratory measurement

The velocity of the longitudinal waves through the samples was measured by using the transit–time method, an ultrasonic–seismic method. In order to calculate the velocity, the transit time through a sample and the length of the sample have to be determined.

The length is measured by means of a slide gauge. Afterwards the sample will be mounted pneumatically between two vertically oriented transceivers (fig. 2.3). The transceivers of the company Deutsch have a spectrum of $0.8 - 3MHz$. Transceiver 1, the transmitter, at the top is supplied by a delta–impulse with an amplitude of $5V$. The

signal is generated by a Tektronix TM 5006 a waveform generator and transferred to the transmitter via a Krohn–Hite 7500 broad band amplifier. Due to the piezo–electric effect the impulse is converted into an elastic wave at the interface of transmitter and sample. The wave travels through the sample and is recorded at transceiver 2, the receiver. There the mechanical wave is converted into a voltage and will be displayed by means of a Tektronix TDS 420 oscilloscope on channel 2. The connection of the transceivers with the sample is improved by using an ultrasonic–contact–agent.

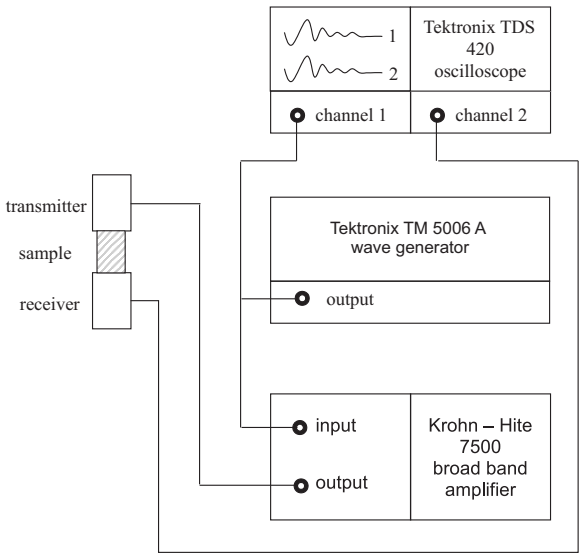

Figure 2.3: Principle sketch of the velocity measurement process

The elapsed time measured between transmitter and receiver on channel 2 compared to the original input signal on channel 1 is the preliminary transit time. In order to get the real transit time without any instrumental influences the zero–offset–time t_0 between transmitter and receiver has to be measured at the beginning of each test series and has to be subtracted from the preliminary transit times.

Subsequently the velocity v of each sample is calculated by means of the ratio of the preliminary transit time t_T minus the zero–offset–time t_0 divided by the sample length l.

$$v = \frac{l}{t_T - t_0} \qquad \left[ms^{-1}\right]$$

2.3 Magnetic Properties

2.3.1 Basic principles of susceptibility

The behavior of a rock sample in a magnetic field can be described by means of its magnetic susceptibility. This magnetic phenomena arises from the motion of electrically charged particles at the atomic scale within the rock constituents. As rocks consist of various minerals the overall magnetic behavior is dependent on the magnetic susceptibility of each component. Regarding this differences three main groups have to be distinguished (Soffel, 1991):

1. Diamagnetism

   All rocks show diamagnetic features. Diamagnetism is only measurable if an external magnetic field is applied. This kind of magnetization is caused by complete electron shells orbiting around a nucleus. Due to the low and negative values of susceptibility in the region of $10^{-5}SI$ the diamagnetism is mostly overprinted by the stronger types of magnetism, para– and ferromagnetism. Diamagnetic susceptibility is the only magnetism independent of temperature.

2. Paramagentism

   This kind of magnetism as well as diamagnetism is only present if an external magnetic field is applied. The electron pairs of such substances are incomplete and uncoupled and start to precess under the influence of a magnetic field and therefore produce a magnetization that has the same direction as the applied field. An increase of the total magnetization occurs as the electron spin of the unpaired electrons causes a partial alignment of the atomic dipole moments. Paramagnetic substances have positive susceptibility values typically around $5 \cdot 10^{-4}$SI for the common rock forming minerals (Tarling & Hrouda, 1993). Therefore paramagnetic substances overprint a low value diamagnetism. Paramagnetic substances are temperature dependent which is given by Curies law.

3. Ferro–, antiferro– and ferrimagnetism

   Substances in which electron spins interact spontaneously (spontaneous magnetization) in a way that individual spin magnetizations have been aligned even in absence of an externally applied field are called ferromagnetic minerals. This magnetic behavior is possible as a result of the existence and properties of magnetic domains (single-domain, multi-domain). Due to different orientations of

intrinsic magnetic moments within magnetic domains three types can be distinguished (fig. 2.4):

- ferromagnetic minerals: parallel oriented intrinsic moments with a resulting macroscopic external moment
- antiferromagnetic minerals: equal but aniparallel intrinsic moments resulting in a zero macroscopic moment
- ferrimagnetic minerals: different antiparallel intrinsic moments of different magnitudes and therefore a resulting external moment

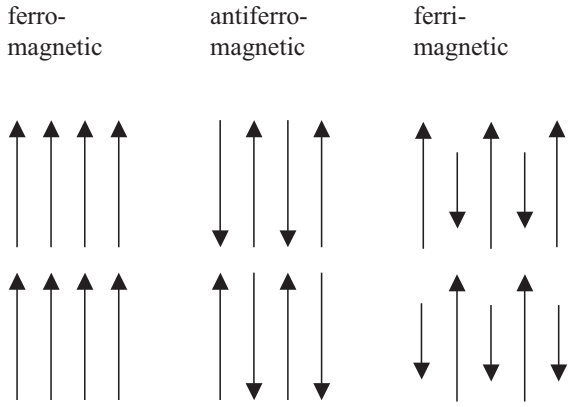

Figure 2.4: Schematic illustration of the orientation of magnetic moments for ferromagnetic, antiferromagnetic, and ferrimagnetic materials (Soffel, 1991)

In case of dia– and paramagnetic substances the effect of magnetization is only present if an external magnetic field is applied. Therefore the strength of the induced magnetization M (magnetization intensity or dipole moment per unit volume) is directly related to the strength of the applied magnetic field H (Schön, 2004):

$$\underline{M} = \kappa \cdot \underline{H} \qquad [Am^{-}1]$$

The susceptibility κ notifies the degree to which a body is able to be magnetized (Telford et. al., 1990).

The strength of magnetization of rocks is dependent on the mineral compound, the grain size, the distribution in the rock sample and their possible alignment (heterogeneity). Due to the high magnetization of ferromagnetic minerals the susceptibility measured in rocks is generally caused by ferromagnetic minerals even by a small amount.

2.3.2 Basic principles of remanent magnetization

Ferro– and ferrimagnetic materials show the phenomenon of remanent magnetization. Remanent magnetization describes the predominant magnetization available depending on the strength of the magnetic field and changes in magnetization in the course of time. The total magnetization M_T is determined by the sum of two vectors, the vector for induced magnetization M_I dependent on the present external field and the vector for remanent magnetization M_R independent of the external field.

$$M_T = M_I + M_R \qquad [Am^{-}1]$$

As ferromagnetic minerals are temperature dependent the magnetization can be changed by heating processes and disappears above a temperature limit value, Curie–Neél level (Schön, 2004).

Rocks show different types of remanent magnetization which are distinguished due to their formation. The natural remanent magnetization NRM is the sum of all types of remanent magnetization available in a rock sample (Schön, 2004) and has a complex influence on the degree of magnetization in amplitude and direction as it is dependent on the mineral content, the magnetic history and the present magnetic field (Telford et. al., 1990). Thermoremanent magnetization TRM is evident when a rock melt passes Curie temperature in the presence of a magnetic field. Chemical remanent magnetization CRM is produced during the formation of a magnetic mineral or if a transition due to weathering occurs. Detrital or depositional remanent magnetization DRM is evident if an oriented deposition of previously magnetized mineral grains under the influence of the terrestrial magnetic field takes place. Further on special types of magnetization are known, isothermal remanent magnetization IRM (e.g. produced by lightnings), viscous remanent magnetization VRM (time effect) and piezo–remanent magnetization PRM (pressure effects).

The degree of magnetization and the direction of the causing magnetic field can be determined and indicate the predominant magnetic field while formation and possible movements of specific rock formations afterwards. Therefore remanence is used to describe paleomagnetic movements and structural conditions (Schön, 2004).

2.3.3 Basic principles of the anisotropy of magnetic susceptibility

The anisotropy of magnetic susceptibility is evident due to the internal rock structure. This feature is described by means of three principal susceptibilities κ_1, the maximum value, κ_2, the intermediate value, and κ_3, the minimum value, which are represented in a susceptibility ellipsoid (fig. 2.5) where the orthogonal axes describe the three parameters. Based on the three principal susceptibilities a detailed description of the magnetic anisotropy can be done by means of parameters.

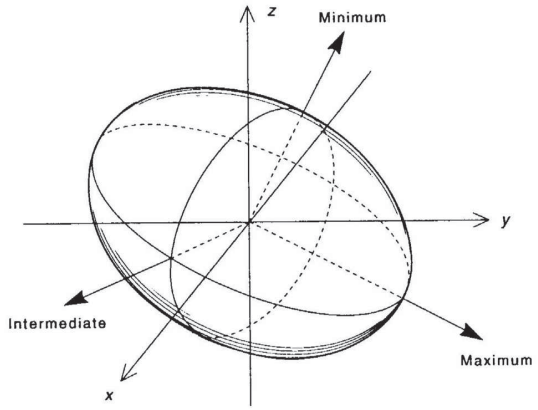

Figure 2.5: The susceptibility ellipsoid defining the susceptibility anisotropy by three orthogonal axes corresponding to the maximum, intermediate and minimum susceptibility value (Tarling & Hrouda, 1993)

The mean susceptibility K_{mean} is given by:

$$K_{\text{mean}} = \frac{\kappa_1 + \kappa_2 + \kappa_3}{3}$$

The degree of anisotropy P is defined by the ratio of the maximum to the minimum susceptibility.

$$P = \frac{\kappa_1}{\kappa_3}$$

The foliation factor F describes a possible alignment of minerals in a specific layer and is defined by the ratio of the intermediate to the minimum susceptibility.

$$F = \frac{\kappa_2}{\kappa_3}$$

The lineation factor L characterizes layers with unidimensional features and is defined by the ratio of the maximum to the intermediate susceptibility.

$$L = \frac{\kappa_1}{\kappa_2}$$

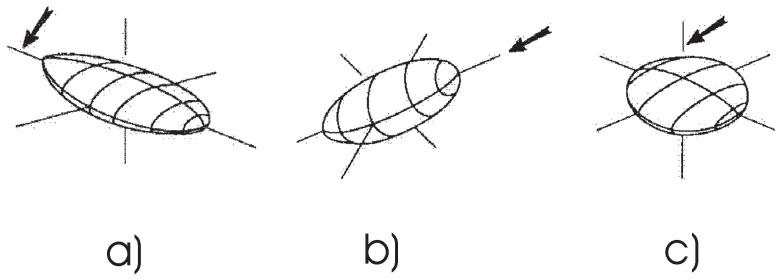

Figure 2.6: Sketch of the three anisotropy structures: a) triaxial shape, b) prolate shape, c) oblate shape (Tarling & Hrouda, 1993)

The internal structure of a rock sample can be described using the stated parameters. Therefore an oblate, prolate or triaxial shape of the susceptibility ellipsoid are distinguishable (fig. 2.6). The prevalent shape is oblate if the foliation factor F is predominant as the prolate shape is given if the lineation factor L is predominant. The triaxial shape is existent if the values for the lineation and foliation factor are equal but not around zero and thus not homogeneous.

2.3.4 Method of laboratory measurement

Measurement of natural remanent magnetization (NRM) with succeeding AF–demagnetization and the anisotropy of isothermal remanent magnetization (IRM)

The remanent magnetization is measured by means of a 2G DC–SQUID magnetometer (fig. 2.7). The DC–SQUID (**S**uperconducting **QU**antum **I**nterference **D**evice) magnetometer is used to measure extremely weak magnetic fields with high accuracy. In order to measure the weak signals the effect of flux quantisation and the Josephson effect are used.

The DC–SQUID magnetometer consists of a superconducter of niobium and two Josephson junctions which divide the supercondcutor into two parts. The junctions are very thin allowing the electrons to pass through. The device is surrounded by a helium reservoir as superconduction occurs only at low temperatures around $4K$ $(-269°C)$. In order to measure the magnetic field intensity of a sample a direct current is induced via the Josephson junctions to the superconductor. This causes a measurable decrease in the electrical voltage which is dependent on the strength of the induced direct current and the compensating flux evident in the superconductor. Hence, a variation in the magnetic field due to diversifying sample properties changes the current in the

Figure 2.7: 2G DC–SQUID magnetometer, paleomagnetic laboratory Gams, University of Leoben, Austria

superconductor and thus the electrical voltage. A DC–SQUID magnetometer can not measure absolute values of the magnetic field intensity, only its changes. Thus, before inserting a sample, the background magnetization is measured and in comparison to this value the magnetic field intensity of a sample is determined.

A DC–SQUID magnetometer is very sensitive to influences of the earth magnetic field. Hence the device is located inside Mu–metal–shieldings which produce a uniform, zero magnetic field.

In order to measure the natural remanent magnetization NRM the samples are inserted into the DC–SQUID magnetometer by means of a specimen slide. Further on, the background magnetization is measured before and after determining the NRM in four spatial directions. The result is corrected considering the sample volume and is displayed by means of a computer program.

An alternating field demagnetization (AF–demagnetization) is done to characterize the magnetic particles evident in the samples. Furthermore, this examination allows a description of possible secondary imprinted magnetic fields. Therefore a stepwise demagnetization process is applied determining the remaining magnetic intensity.

By using a pulse magnetizer the isothermal remanent magnetization IRM is examined. The 2G Pulse Magnetizer operates by charging capacitators with a low current, then sending a high current through a solenoid to generate a pulsed magnetic field. The generated field used in this survey has an intensity of 2.7 T. The IRM was imprinted in six spatial directions and measured by using the DC–SQUID magnetometer.

Measurement of magnetic anisotropy (AMS)

The Kappabridge KLY–2 (Geofyzika Brno) is used to measure the magnetic susceptibility and the anisotropy of the rock samples. The device is operated by an alternating current with a frequency of $920Hz$ and a magnetic field with the strength of $300Am^{-1}$. It consists of two units, the pick up unit and the measuring unit (fig. 2.8).

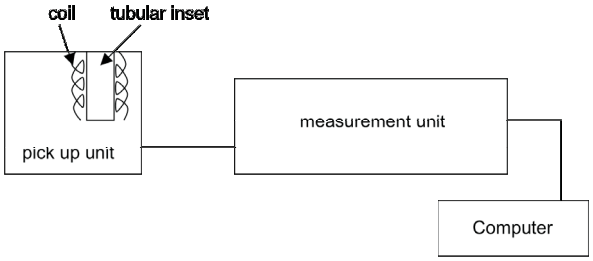

Figure 2.8: Schematic illustration of the Kappabridge KLY–2, Geofyzika Brno

The pick up unit comprises a tubular inset which is surrounded by a coil. The tubular inset acts as placeholder for the sample holder and the coil induces the external magnetic field which allows to determine the magnetic susceptibility of a rock sample. The specimen is placed inside the tubular inset by means of a sample holder. The magnetic influence of the sample holder is measured before starting the test series and is removed when executing the calculations after the measuring process. The measuring unit records the values, displays them on a digital screen and transmits them to a computer where further calculations are carried out.

For the purpose of measuring the anisotropy in an accurate way the specimen is measured in 15 different spatial positions (fig. 2.9). These positions are labeled by dots and arrows on the outside of the sample holder. The measuring process is started by inserting the rock sample into the sample holder in the first position. Subsequently the sample holder is put inside the tubular inset and the measurement starts. This process is repeated for all 15 spatial positions until finally the data set for the specimen is complete.

The standard error for the residuals has to be beyond a threshold of 10 to be certain the measurement is accurate. By means of a computer program calculations on the mean susceptibility K_{mean}, the degree of anisotropy P, the foliation factor F, the lineation factor L and shape parameters are carried out. Further on, the specimen and the geographical directions of the susceptibility ellipsoid are calculated which allows to draw conclusions on the shape and orientation of the magnetic anisotropy of a rock sample, the processes of creation and the affecting magnetic field.

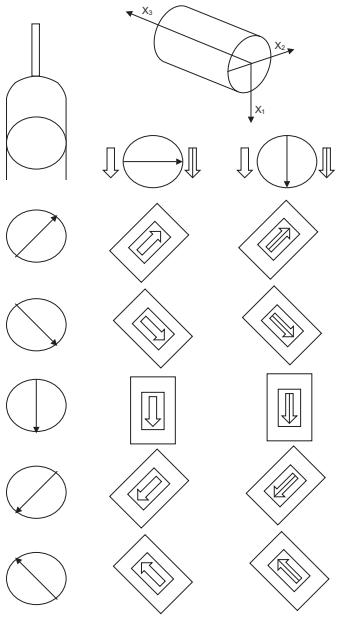

Figure 2.9: Schematic illustration of the 15 spatial directions

In order to get proper results the pick–up unit is positioned in a magnetically undisturbed environment with a constant temperature. The measuring unit and the computer are placed as far away from the pick–up unit as possible to avoid any disturbance.

2.4 Electrical Properties

2.4.1 Basic principles of electrical properties

The electrical properties of rock samples are defined by the primary properties of electrical conduction (charge transport). Therefore the current density j is defined by the product of the electric conductivity σ and the electric field strength E (Schön, 2004).

$$\vec{j} = \sigma \cdot \vec{E} \qquad \left[A/m^2\right]$$

To describe the electrical properties of rocks in geophysics the specific resistivity ρ is used which is defined by the reciprocal value of the conductivity σ (Schön, 2004).

$$\rho = \sigma^{-1} \qquad [\Omega m]$$

As the various rocks show different conductivities the materials are subdivided in respect to their ability to conduct. Hence, conductors ($\sigma > 10^5 Sm^{-1}$), semiconductors

($10^5 > \sigma > 10^{-8} Sm^{-1}$) and insulators ($\sigma < 10^{-8} Sm^{-1}$) are differentiated (Schön, 2004).

The electrical conductivity in rocks and minerals is dependent on the kind of conduction and the prevailing temperature. Therefore the following types are important (Schön, 2004):

- Metallic conduction (native metals as copper, gold and graphite)
- Electronic semiconduction (minerals like ilmenite, magnetite, pyrite and galena)
- Electrolytic conduction
  - Solid electrolytes (ionic crystals as most rock–forming minerals): The transfer of electric current occurs by motion of ions through a crystal lattice.
  - Electrolyte water solution (pore–water bearing in rocks causing the dominant electric current transfer)

An overview on the electrical conductivity of the common rock–forming minerals shows a very high resistivity or a low conductivity with a comparable result for absolute dry rocks. If a porous or fractured rock is water–bearing the electrolytic conductivity is enhanced due to the electrical conductivity of the water itself and the interaction between solid and fluid components. Thus, dense, pore and fracture free rocks or absolute dry rocks are easy to distinguish from porous or fractured rocks (Schön, 2004).

Dense, pore and fracture free rocks or absolute dry rocks occur infrequently in the near surface crust. The conduction is controlled by matrix properties which results in three significant observations, high resistivity values, a temperature and a pressure dependence. Therefore it can be stated that an increase in pressure causes a decrease of the specific resistivity as the fractures will be closed. In case of temperature it is more difficult as the conductivity is dependent on the various conduction mechanism caused by various activation energies (Schön, 2004).

The electrical conductivity of porous and fractured rocks is mainly controlled by the features of the pore fluid which is an electrolyte. The conductivity of the solid matrix is therefore in most cases negligible besides in the presence of vein type ores, rich disseminated ores or graphite (Schön, 2004).

In order to analyze the anisotropy of rock samples the electrical conductivity or the specific resistivity is measured. The anisotropy is caused by preferred orientations of conducting minerals or accessories (e.g. ores, graphite), the preferred orientation of

the wet or water saturated pores and cracks or fine layering of rock components with different conductivity (clay–sand "sandwich–layering ") (Schön, 2004). For layered rocks Keller and Frischknecht (1966) invented the coefficient of anisotropy A_ρ which is defined by the radical of the ratio of the resistivity perpendicular to the layer $\rho_\perp$ to the resistivity parallel to the layer $\rho_{\shortparallel}$.

$$A_\rho = \left(\frac{\rho_\perp}{\rho_{\shortparallel}}\right)^{\frac{1}{2}}$$

The resistivity perpendicular to the layer plane is given by

$$\rho_\perp = \frac{\sum_i (\rho_i \cdot h_i)}{\sum_i h_i}$$

with the resistivity ρ_i of the i–th layer and its thickness h_i. The resistivity parallel to the layer plane is defined by

$$\rho_{\shortparallel} = \frac{\sum_i h_i}{\sum_i \left(\frac{h_i}{\rho_i}\right)}.$$

2.4.2 Method of laboratory measurement

The specific resistivity of each sample is determined by means of a resistivity measurement (fig. 2.10). For this purpose the geometry of the sample has to be measured as well as the electrical voltage which flows through the sample when an electric current is applied.

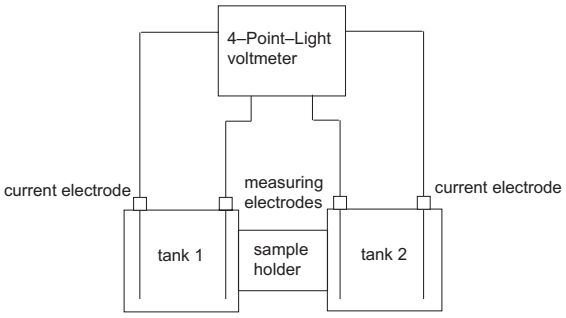

Figure 2.10: Principle sketch of the resistivity measurement process

The geometry of the cylindrical samples is measured by means of a slide gauge and is taken into consideration by the geometry factor. It is defined by the ratio of the area of the circle $r^2\pi$ to the length l of the sample.

$$F_G = \frac{r^2\pi}{l} \qquad [m]$$

Afterwards the electric voltage is measured by means of a 4–Point–Light voltmeter (Lippmann Geophysikalische Messgeräte). The instrument transmits an electric current in the range of $100nA - 10mA$ in six tenner ranks with a frequency of $8.33Hz$.

The saturated samples are mounted in a connecting part of two tanks filled with a $0.058\%weight$ NaCl solution. In order to allow an adaption between the pore fluid of the saturated sample and the solution in the tanks a one hour period of rest is kept to. After this period the conductivity in each tank is measured as well as the temperature. Subsequently a platinum net and a platinum pin electrode are put in each tank where the net electrodes supply the electrical current and the pin electrodes measure the electric voltage.

The specific resistivity is calculated by means of Ohms law which is defined by the ratio of the electric voltage U to the electric current I. In order to take the geometry into consideration the geometry factor F_G is multiplied.

$$\rho = \frac{U}{I} \cdot F_G \qquad [\Omega m]$$

Chapter 3

Bad Gleichenberg

3.1 Geology

The Styrian Basin located in the south-east of Austria (fig. 3.1), is one of the Neogene basins created on the edge of the eastern part of the alps (Tollmann, 1985). At the end of the young Alpidic orogeny an eastward directed extension causes a continental, lateral escape towards the Pannonian region which is essential to the formation of the Styrian Basin. This process is a consequence of the collision of the Apulian and European tectonic plates which is crucial to the forming process of the Alpine mountain range (Ebner & Sachsenhofer, 1991). Due to the shearing faults caused by the orogenesis, the creation of the Neogene basins amongst the Austrian Alps show a direct connection to the Innercarpathian Region (Ebner & Sachsenhofer, 1991). Therefore the Styrian Basin can be seen as part of the Pannonian Basin which enlarges towards south-east. Starting in the Ottnangian (18.1–17.2 mya)/Karpatian (17.2–16.5 mya) age, a two-phase evolutionary history forms the basin. The first phase is defined by a large subsidence rate linked with synsedimentary disjoining tectonics which is caused by the extension of the crust and the continental escape. Secondly, a geothermal process lasting up to the point is crucial (Ebner & Sachsenhofer, 1991). Thus the Styrian Basin is the consequence of a thinning crust of the Alps above the mantle. This causes a cave–in of the Pannonian Field and the surrounding basins. Therefore the forming process is not a destructive one but a reaction to flexure (Tollmann, 1985).

The boundaries to the Styrian Basin are due to the evolutionary history, enforced by almost N-S striking tectonic faults (fig. 3.2). The Südburgenländische Schwelle in the south-east, which takes a SW-NE course, defines the boundary between the Styrian and the West-Pannonian Basin. The basin is bordered further on by the Possruck in

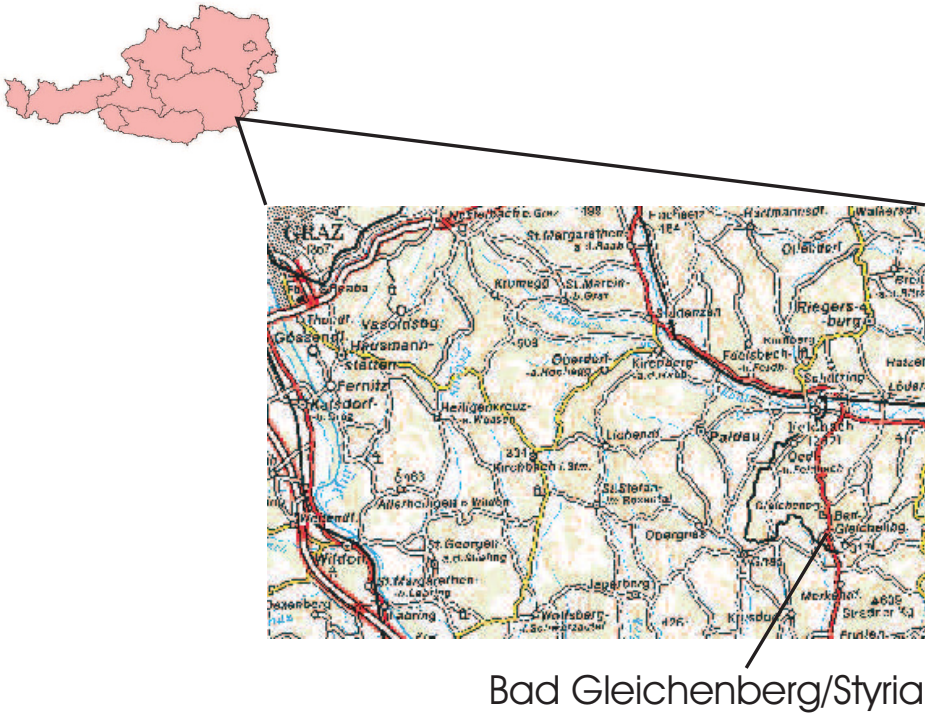

Figure 3.1: Sketch of Austria with indication of the drill location in Bad Gleichenberg in the south–east of the federal state of Styria (Austrian Map 3D).

the south-west, the Koralpenzug in the western part, the Geschriebenstein, Buckelige Welt and Wechsel in the north-east and finally the Masenbergstock and the Paleozoic Grazer Bergland in the north (Tollmann, 1985).

The Styrian basin is split into two main parts which are known as the west and the east Styrian basin (fig. 3.2). The western part which is smaller in area and with a depth of about 800m, is separated from the eastern one by the Sausal- or Mittelsteirische Schwelle. The eastern part, as the larger one, has a depth of about 3000m and is once more subdivided into three basins. Next to the west Styrian basin is the Gnaser basin. The Auersbacher Schwelle defines the borderline to the Fehringer basin. Further on to the east the Fehringer basin is separated by the Söchauer Schwelle from the Fürstenfelder basin (Tollmann, 1985).

The sedimentary filling of the basins started about 20 million years ago during the Miocene epoch (23–11.6 mya) as an interbedded strata mainly of sand and alternating clay and rubble layers. This formation is caused by marine, limnic and fluviatil accumulations (Fritz, 2002). The basis of the western part of the Styrian Basin consists of rocks of the Paleocene period of the Upper Austroalpine. Going on to the north

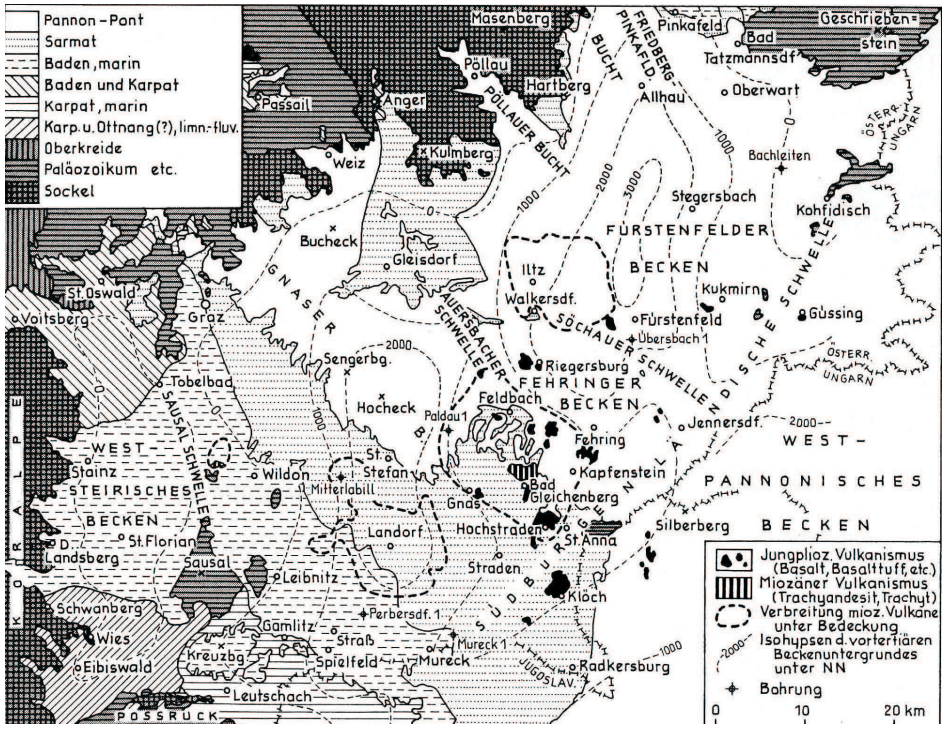

Figure 3.2: Map of the Styrian Basin illustrating the west and east Styrian basin as well as the subdivision of the east Styrian basin into the Gnaser basin, the Fehringer basin and the Fürstenfelder basin. Furthermore the separation by means of the various barriers is indicated. Drawn by K. Kollmann in Tollmann (1985).

eastern part, the subsurface is made up of rocks of the Middle Austroalpine (Tollmann, 1985).

The shift sequence within the basin starts in the Ottnangian age (18.1–17.2 mya). At the base Ferralsol is predominately found which is followed by a laminated limnic series with interbedded bituminous marl (Ebner & Sachsenhofer, 1991). The top is formed by layers of conglomerate (Ebner & Sachsenhofer, 1991). This period is free of volcanic activity (Tollmann, 1985).

The Karpatian age (17.2–16.5 mya) is characterized by the upcoming volcanic activity. This characteristic of the Styrian Basin is part of the out bounding volcanic arc of the Innercarpatic Volcano Belt (Tollmann, 1985). The volcanic activity occurs in three distinctive periods. The oldest one appears in the Karpatian age and lower Badenian age (16.5–12.8 mya) as sub-alkaline–alkaline type represented by trachyandesite, andesite, shoshonite and dazite with representatives next to Bad Gleichenberg, Paldau, Walkersdorf, Weitendorf and Kollnitz (Ebner & Sachsenhofer, 1991). As a result shield volcanoes were formed with a height of about 1200m spread over an area

of $600km^2$. Nowadays all of them are buried by sediments except the Gleichenberger Kogel next to Bad Gleichenberg which is visible at the surface. This kind of volcanism described above is attached to intense extension, strike-slip and subsidizing tectonic events (Ebner & Sachsenhofer, 1991). Subsequent basaltic eruptions take place in the Sarmatian and Pannonian Age marked by alcaline-olivine-basalt, trachydolerite und olivine-tholeiite (Ebner & Sachsenhofer, 1991). The location of this volcanic period is the Landseer Bucht next to Oberpullendorf-Stoob and Pauliberg (Ebner & Sachsenhofer, 1991). Finally, the youngest volcanic activity with basaltic and Na-accentuated lava occurs in the Plio- (5.3–1.8 mya)/Pleistocene (1.8 mya–100000 ya) epoch, which is defined by basaltic lava flows, shield volcanoes and filled pipes. This volcanic period is present in the north at the Riegersburg and in the south at Klöch which is interpreted as caldera.

At the crossover of the Karpatian to the Badenian Age (16.5–12.8 mya) the marine transgression spreads all over the Styrian Basin. Hence a consistent sedimentation of all basins started. The volcanic activity is still powerful with a starting shift towards the north when reaching the end of the Badenian age (Ebner & Sachsenhofer, 1991).

At the start of the Sarmatian age (12.8–11.6 mya) a short period of transgression occurs. Simultaneously, a semi-enclosed sea is separated from the Paratethys. This development causes another consistent sedimentation affected by brackish water. The volcanic activity during this epoch with its basaltic eruptions has its centers near Oberpullendorf–Stoob in the Landseer Bucht and Pauliberg. In this age the volcanism ends and the area is flooded by the sea. The Gleichenberger Kogel is the only one which overtops the sea level (Ebner & Sachsenhofer, 1991).

In the beginning of the Pannonian (11.6– ∼7.8 mya), the water is still brackish and further regression occurs. The Pannonian is classified by five groups, A–E. Due to the regression process there is no Pannonian A, thus the clastic sediments of the Pannonian B and C show the first evidence of the Pannonian Age (Ebner & Sachsenhofer, 1991). Further on an interbedded strata of brash with sand, clay or cole bearing layers occurs in the Pannonian C. This kind of brash is transported by rivers originating in the north-west of the Styrian Basin (Tollmann, 1985). Finally the Pannonian D and E shows another interbedded strata with sand, clay and gravel (Ebner & Sachsenhofer, 1991).

The Pontian Age (∼7.8–5.3 mya) has its only occurrence in the eastern part of the Styrian Basin and is represented by lignite formations.

The last sedimentary input to the Styrian Basin takes place in the Pliocene Epoch

(5.3–1.8 mya). This epoch is characterized by the basaltic volcanism which is documented by three locations of eruption in Klöch, Steinberg, Hochstraden and additional ∼30–40 pipes of tuff. This volcanic activity is the last and youngest occurring in the Styrian Basin. The volcanic eruptions are buried below layers of sediments which are formed by changing river beds created in subtropical climate conditions (Ebner & Sachsenhofer, 1991).

The drill core investigated within this survey is located in Bad Gleichenberg, Styria and was sinked into the Miocene volcanic structure dated back into the Karpatian and lower Badenian age. A K/Ar–dating gives an age of 16 ± 0.9mya respectively 15.5 ± 0.1mya. The structure is characterized as shield volcano which is ,besides the outcrop in Bad Gleichenberg, buried below Sarmatian and Pannonian sediments. The lithologies within the volcanic structure comprise a broad variety as latite, quarzitic latite, trachyte, trachyandesite, dazite and shoshonite (Belocky et. al, 1996). The core pierces through various layers which are listed in tab. 3.1.

sample ID	depth [m]	lithology	total number of samples	samples	
				axial	radial
137	137	latitic lava	3	1	2
194	194	latitic lava	2	1	1
237	237	tuff – alterated tuff	4	2	2
288	288	tuff – alterated tuff	4	2	2
345	345	minor alterated lava	4	2	2
403	403	minor alterated lava	3	1	2
453	453	latitic lava	2	1	1
501	501	latitic lava	6	3	3
552	552	tuff – alterated tuff	4	2	2
588	588	alterated pseudo-breccia	2	1	1
651	651	latite	6	3	3
654	654	latite	4	2	2
705	705	fresh latite	6	3	3
762	762	fresh latite	6	3	3
785	785	alterated pseudo-breccia	4	2	2
842	842	latitic lava	4	2	2
Σ			**64**	**31**	**33**

Table 3.1: Listing of the sample ID with depth indication [m], lithology characterization after Belocky et. al (1996), total amount of samples as well as the distribution of axial and radial samples.

3.2 Sample Preparation

The drill core is provided by Landesmuseum Joanneum Graz and was drilled in 1981 in Bad Gleichenberg. The core reaches a depth of 900m. In order to survey all possible lithologic zones, core samples were taken in intervals of about 50m starting with the first sample at a depth of 137m to the final depth level at 842m.

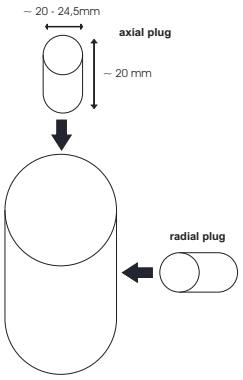

Figure 3.3: Schematic diagram of the sample (plug) preparation with directional indication (axial and radial). The axial and radial plugs are drilled alternate in order to secure a balanced investigation.

The drill core is cut into two halves by means of a diamante cutting disc as one half has to be stored for reference purpose. The second half is used to prepare cylindrical shaped samples (plugs) with a diameter of 2.54 cm (= 1 inch) and a length of about 2 cm (fig. 3.3). Before drilling the axial and radial specimen, the core was sliced by means of a diamond cutting disc. The plugs were drilled by means of a diamond drill bit. The three working steps are shown in fig. 3.4.

Figure 3.4: Sample 654 illustrates the three preparation steps: 1) halved drill core, 2) ∼3cm core slices and 3) plugs with a length of ∼20mm and a diameter of 20–25.4mm.

The samples were used to measure several petrophysical parameters. Due to problems during sample preparation and measurability not all samples could be measured

with each method. Hence, only the magnetic measurements were applied to the samples 237, tuff, and concerning samples 288 and 345 the compressional velocity in dry condition was not determined.

3.3 Results

3.3.1 Density and Porosity

The density and porosity data were obtained by applying the Archimedes‘ principle. The results for bulk density vary in the range of 2.08 to 2.65 g/cm^3 with a standard deviation of ±1.9% and the grain density data shows values between 2.52 and 2.74 g/cm^3 with a standard deviation of ±0.7%. The porosity data vary in the range of 2.71 and 25.91%. The standard deviation is given with a percentage of ±13.7% calculated for each value to be 100%.

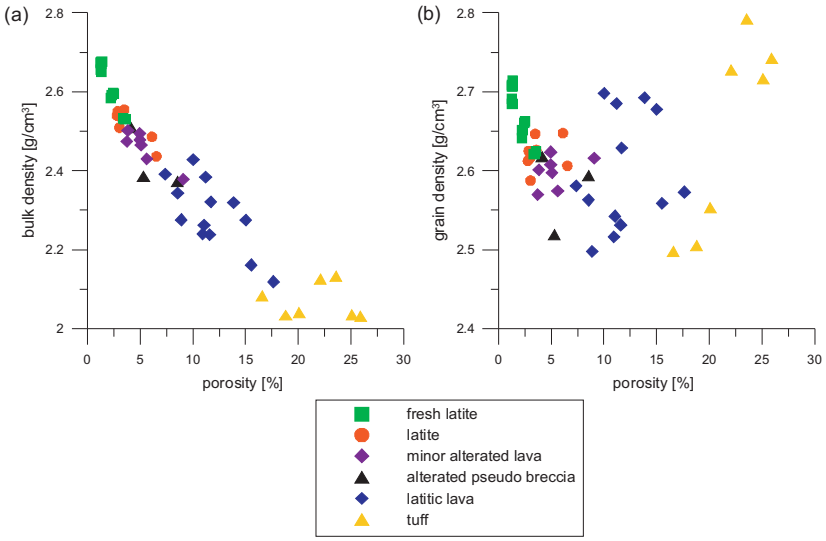

Figure 3.5: (a)Plot of bulk density [g/cm^3] versus porosity [%]. The porosity values decrease with increasing bulk density; (b) Cross plot of grain density [g/cm^3] versus porosity [%]. In terms of grain density versus porosity the same overall trend is given as for bulk density versus porosity. Outliers occur within the lithologies of latitic lava and tuff.

The cross plot of bulk density versus porosity yields a negative correlation, hence, the bulk density decreases with increasing porosity values (fig. 3.5a). Moreover a distinction of the investigated lithologies is obvious. The fresh latite has values for bulk density in the range of 2.53 to 2.68 g/cm^3 and therefore the lowest in porosity between 1.24 and 3.57 %. The contrary to fresh latite is tuff indicated by a bulk density

between 2.03 and 2.13 g/cm^3 and porosity values in the range of 16.57 and 25.91 %. Latite follows next after fresh latite and has values between 2.44 and 2.55 g/cm^3 for bulk density and 2.85 and 6.53 % for porosity. After this, minor alterated lava follows with bulk density results in the range of 2.43 to 2.50 g/cm^3 and porosity between 3.72 and 9.08 %. Alterated pseudo breccia plots within the ranges of 2.37 and 2.51 g/cm^3 for bulk density and between 4.14 and 8.54 % for porosity. Considering the latitic lava a wide range for both density (2.12 and 2.43 g/cm^3) and porosity (7.36 and 17.63 %) is observed.

In terms of grain density versus porosity, generally the same overall trend as described in case of bulk density versus porosity occurs (fig. 3.5b). The negative correlation is also evident in this cross plot, except that grain density of latitic lava spreads out towards high values (2.50 to 2.70 g/cm^3) although indicated by high porosity values. The same is observed for a group of tuff samples with the highest values for grain density (2.79 g/cm^3). Apart from that the sequence in lithologies from fresh latite to tuff is also observed.

3.3.2 Electrical properties

Results of the specific electrical resistivity measurement versus porosity are plotted in figure 3.6. The values for electrical resistivity vary between 20 and 1015 Ωm. The accuracy of the applied method and the average deviation with a value of $\pm 1\%$ is determined by means of repeated measurements.

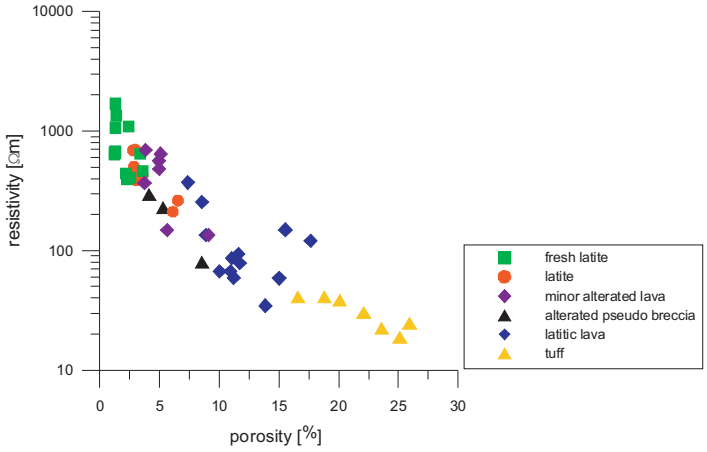

Figure 3.6: Plot of the average electrical resistivity results [Ωm] versus porosity [%] with indication of the various lithologies observed. The investigation shows groupings of the surveyed lithologies.

The electrical resistivity decreases with increasing porosity values. Thus, tuff shows the lowest value in electrical resistivity (18.70 to 41.22 Ωm) and the highest values in porosity (16.57 to 25.91 %). The contrary is valid for the fresh latite as the electrical resistivity is indicated by the highest (393.81 to 1688.82 Ωm) and the porosity by the lowest values (1.24 to 3.57 %) observed. Starting from this point a continuous decrease in electrical resistivity and a continuous increase in porosity differentiate the available lithologies significantly. Latite is indicated by electrical resistivity results in the range of 211.15 and 697.49 Ωm. Following latite, minor alterated lava has resistivity values between 134.92 and 695.92 Ωm. Alterated pseudo breccia and latitic lava show the same range in terms of electrical resisitvity between 34.65 and 370.87 Ωm. The differentiation occurs due to the variation in porosity whereas alterated pseudo breccia is indicated by lower porosity values.

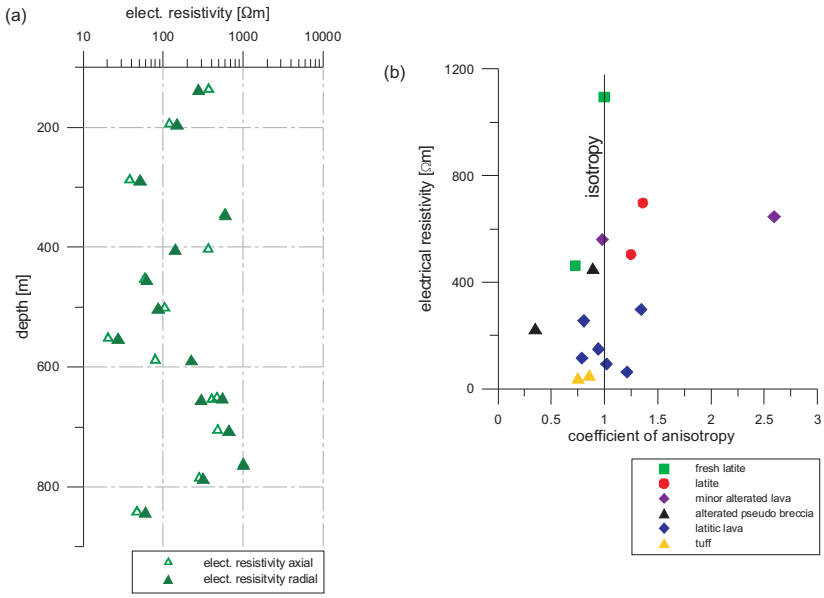

Figure 3.7: (a) Plot of the average electrical resistivity results [Ωm] in axial and radial direction versus depth [m]; (b) Cross plot of electrical resistivity versus the coefficient of anisotropy. The results plot randomly and a correlation of lithology and coefficient of anisotropy is uncertain.

Subsequent to the analysis of the electrical resistivity further investigations by means of anisotropy have been carried out. The samples were measured in axial and radial direction (fig. 3.7a) and afterwards the coefficient of anisotropy was calculated. A coefficient of anisotropy of 1.0 indicates isotropy. Considering the obtained values the direction of preferred electrical conductivity is neither axial nor radial (fig. 3.7a). The ratio of the coefficient of anisotropy plotted versus the electrical resistivity yields

a significant anisotropy, but a correlation with the lithology groupings is uncertain (fig. 3.7b).

3.3.3 Magnetic properties

The magnetic properties of the samples were determined by measuring the anisotropy of the magnetic susceptibility (AMS) and the natural remanent magnetization (NRM).

The mean magnetic susceptibility is determined by means of a Kappabridge KLY–2 and varies in the range of 285 to $14974 \cdot 10^{-6} SI$ with a standard deviation of $\pm 14.3\%$. A general trend that an increase in mean susceptibility correlates with a decrease in porosity is observed. Fresh latite is indicated by the highest values in mean susceptibility (11910 to $17150 \cdot 10^{-6} SI$) and the lowest results for porosity (fig. 3.8a). Minor alterated lava has mean susceptibility values in the range of 7452 and $15730 \cdot 10^{-6} SI$ whereas the susceptibility of latite plots between 6037 and $8665 \cdot 10^{-6} SI$. As latite is indicated by slightly higher porosity values than minor alterated lava a change in the sequence of lithology described in terms of bulk density, grain density and electrical resistivity versus porosity occurs. The samples of alterated pseudo breccia and latitic lava plot within the same range for mean susceptibility (350 to $4305 \cdot 10^{-6} SI$).

The NRM values vary in the range of $8.70 \cdot 10^{-3}$ and 1.39 A/m. The results plotted versus mean susceptibility allow a distinction of the investigated lithologies only in terms of mean susceptibility as the NRM values scatter (fig. 3.8b). In case of fresh latite a range of $9.85 \cdot 10^{-1}$ and 1.23 A/m is observed which is also valid for minor alterated lava. However, latite varies between $4.06 \cdot 10^{-2}$ and $1.04 \cdot 10^{-1}$ A/m. Considering the results for alterated pseudo breccia, latitic lava and tuff one group is observed for both NRM and mean susceptibility values. The variation occurs in the range of $9.47 \cdot 10^{-2}$ and $1.09 \cdot 10^{-1}$ A/m for NRM and between 350 and $4305 \cdot 10^{-6} SI$ for mean susceptibility.

Plotting the mean susceptibility results versus the degree of anisotropy gives a first overview on the anisotropy behaviour of the investigated samples (fig. 3.9a). The values for the degree of anisotropy plot between 1.004 and 1.059 and indicate a very weak anisotropy. As stated above the investigated lithologies show variations in mean susceptibility. In terms of anisotropy degree a correlation is observed as fresh latite, latite and minor alterated lava show values for the anisotropy degree between 1.014 and 1.038 whereas alterated pseudo breccia, latitic lava and tuff spread out in the range of 1.005 and 1.038 with two outliers within the latitic lava lithology.

Furthermore, the lineation factor is plotted versus the foliation factor (fig. 3.9b). The solid line within the plot specifies the triaxial shape and besides that indicates the

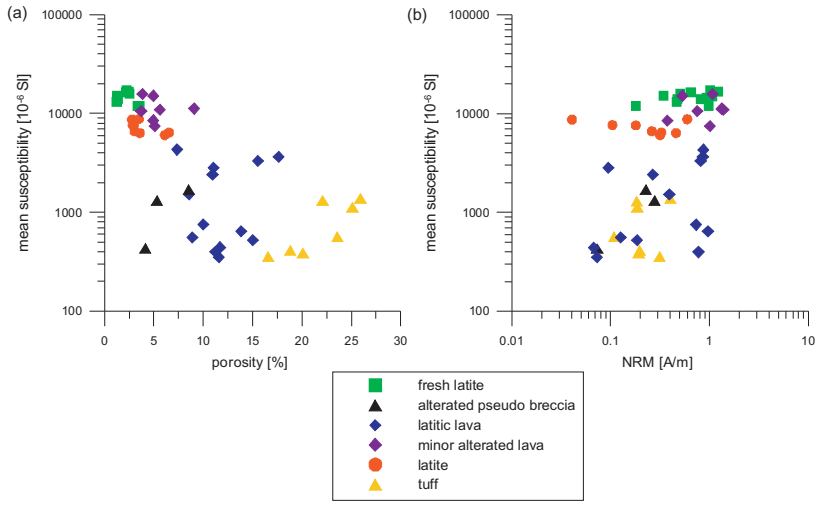

Figure 3.8: (a) Cross plot of the mean susceptibility [$10^{-6}SI$] versus porosity [%]. The mean susceptibility values show the trend to increase with decreasing values in porosity; (b) Plot of mean susceptibility [$10^{-6}SI$] versus NRM [A/m]. A distinction of the investigated lithologies in terms of NRM is difficult, as the results scatter.

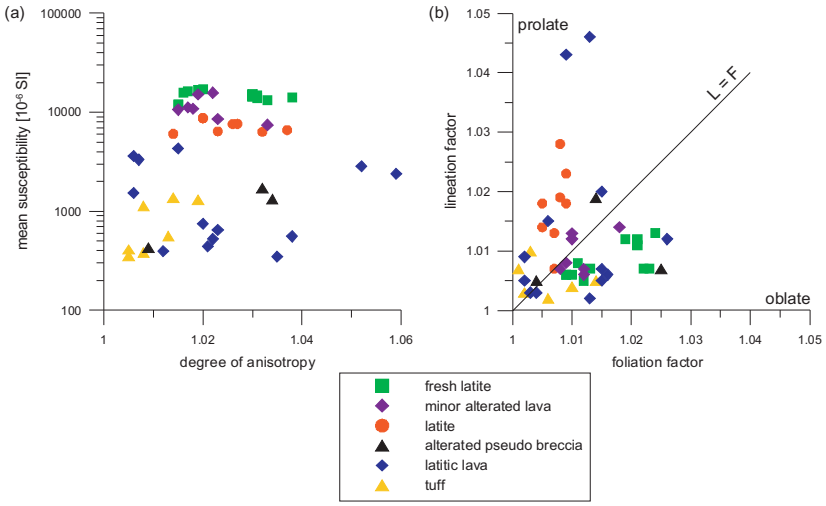

Figure 3.9: (a) Cross plot of mean susceptibility [$10^{-6}SI$] versus degree of anisotropy. The results plot randomly and thus, it is not possible to correlate the results of mean susceptibility with the degree of anisotropy; (b) Plot of foliation factor versus lineation factor. The solid line indicates triaxial shape and acts as borderline between oblate and prolate shape. The results scatter within the diagram and therefore no preferred shape is observed.

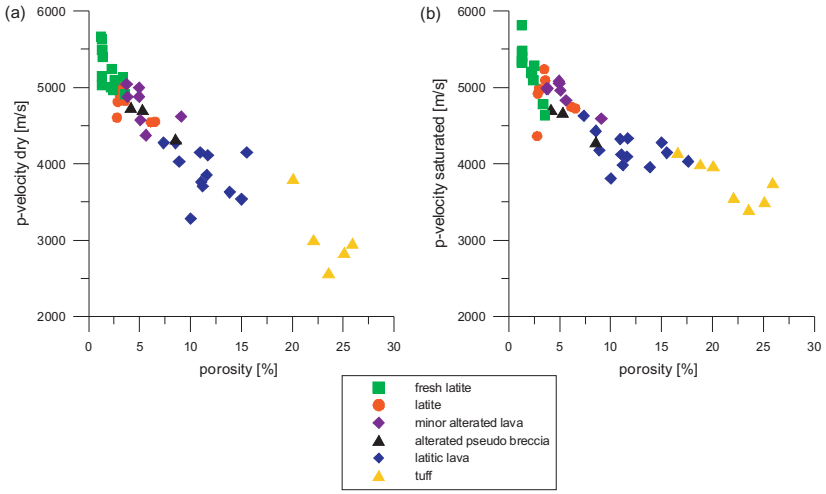

Figure 3.10: (a) Cross plot of p-velocities measured in dry condition [m/s] versus porosity [%]. A decrease in p-velocity correlates with an increase in porosity values; (b) Cross plot of p-velocities measured in saturated condition [m/s] versus porosity [%]. The same trend as observed in terms of the dry condition measurement is valid with slightly increased p-velocity results.

boundary between prolate and oblate shape. The values for the foliation factor vary between 1.001 and 1.026 and for the lineation factor in the range of 1.001 to 1.046. In general the measured values scatter within the diagram and thus, no preferred shape, e.g. prolate or oblate, is obvious. However, two lithologies are indicated by significant shape types. Fresh latite shows an oblate shape with a foliation factor in the range of 1.009 and 1.024 and a lineation factor between 1.005 and 1.013. A prolate shape occurs in case of latite whereas the foliation factor has a range of 1.005 and 1.009 and the lineation factor varies between 1.007 and 1.028.

3.3.4 Elastic properties

The ultrasonic compressional velocities were obtained applying an ultrasonic transit–time measurement method. The equipment allows an accuracy for the offset–time of 0.04 μs as this is the smallest measurement grid. In order to get a good characterization of the surveyed drill core the samples were measured in two conditions, dry and saturated. Some of the dry samples could not be measured due to e.g. high porosity or fragility. Nevertheless, the overall trend of the saturated samples is comparable to the trend given by the dry samples.

The p-velocity values obtained measuring the samples in dry condition vary in the range of 2708 and 5566 m/s with a standard deviation of $\pm 1.5\%$. Comparing the p-

velocity versus porosity an increase in porosity correlates with a decrease in p-velocity values (fig. 3.10a). The highest values in p-velocity (4910.71 to 5670.10 m/s) and thus, the lowest porosity (1.24 to 3.57 %), occurs for fresh latite. Latite is indicated by slightly lower values in p-velocity (4545.45 to 4969.88 m/s) and higher porosity (2.85 to 6.53 %). In case of minor alterated lava and alterated pseudo breccia the p-velocity (4326.92 to 5045.87 m/s) as well as the porosity (3.72 to 9.08 %) vary in the same ranges. Latitic lava has p-velocity values in the range of 3280.32 to 4150.94 m/s and the porosity varies between 7.36 to 17.63 %. Tuff is indicated by the lowest p-velocity results (2577.74 to 3810.62 m/s) and the highest porosity values.

The results of the compressional velocity measurement for the saturated samples vary in the range of 2577 and 5488 m/s with a standard deviation of $\pm 1.7\%$ (fig. 3.10b). In terms of the p-velocities measured in saturated condition plotted versus porosity the same trend as well as the same lithology sequence as described for the measurement in dry condition occurs. A difference is given as the p-velocities are slightly increased.

In order to specify the characterization of the various lithologies the results have been analysed by means of anisotropy measurements in axial and radial direction (fig. 3.11a and 3.12a). By calculating the ratio between axial and radial direction the coefficient of anisotropy is obtained. A deviation from a value of 1.00, which indicates isotropy, allows a characterization of the anisotropy degree. Although for most of the samples a significant anisotropy degree is found the grouping and sequence determined in terms of the cross plots of the absolute values is not observed (fig. 3.11b and 3.12b) as the coefficient of anisotropy for both measurement conditions plots randomly.

A summary of all investigated petrophysical parameters for the lithologies of fresh latite, latite and minor alterated lava is plotted in tab. 3.2. Tab. 3.3 lists the results for the lithologies of alterated pseudo breccia, latitic lava and tuff. The tables indicate the mean value, the respective standard deviation and the minimum and maximum value.

3.4 Discussion

The drill core of Bad Gleichenberg was sinked into a geological structure verified as shield volcano due to previous studies and accomplished geological mapping (Tollmann, 1985; Belocky et. al., 1996). After the forming of the volcano a subduction took place which was followed by a sedimentary refill but no further major tectonic events are traced (Ebner & Sachsenhofer, 1991, Tollmann, 1985). Hence, nowadays most of the

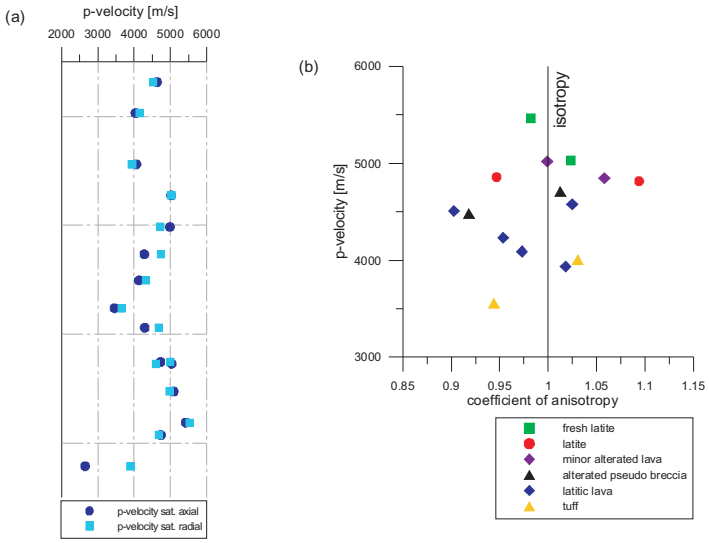

Figure 3.11: (a) Plot of the p-velocities measured in saturated condition in axial and radial direction [m/s] versus depth [m]; (b) Plot of the p-velocity measured in saturated condition versus the respective coefficient of anisotropy. The anisotropy is significant, but a correlation of the observed lithologies with a certain coefficient of anisotropy is uncertain.

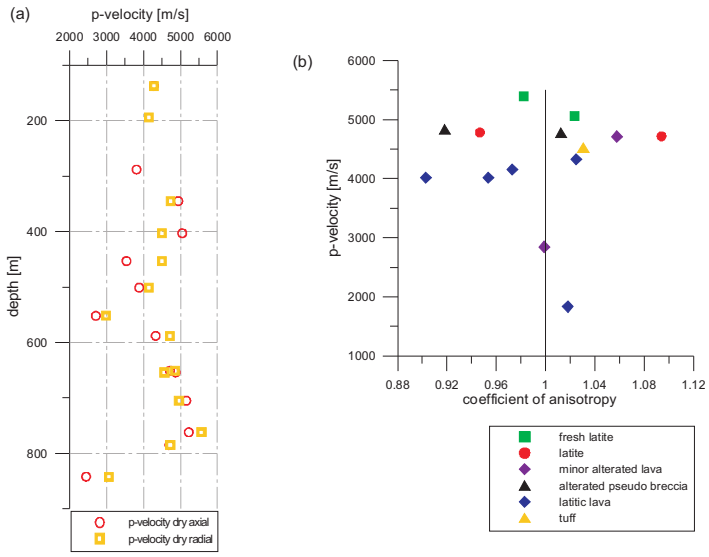

Figure 3.12: (a) Plot of the p-velocities measured in dry condition in axial and radial direction [m/s] versus depth [m]; (b) Plot of the p-velocity in dry condition versus the coefficient of anisotropy for the various lithologies. The grouping and sequence of the lithologies found in terms of absolute values is not observed.

	fresh latite			latite			minor alterated lava		
	mean value	std deviation	min/max	mean value	std deviation	min/max	mean value	std deviation	min/max
bulk density [g/cm3]	2,610	0,050	2.53 / 2.68	2,520	0,040	2.44 / 2.55	2,460	0,040	2.43 / 2.51
grain density [g/cm3]	2,690	0,020	2.62 / 2.71	2,620	0,020	2.59 / 2.65	2,600	0,020	2.52 / 2.62
porosity [%]	2,720	1,320	1.24 / 3.57	3,900	1,320	2.85 / 6.53	5,320	1,660	3.72 / 9.08
electrical resistivity axial [Ωm]	746,11	437,98	393.81 / 1688.82	445,9	156,52	211.15 / 688.43	515,43	136,36	366.48 / 695.98
electrical resistivity radial [Ωm]	839,76	345,3	460.93 / 1343.23	452,26	149,73	262.44 / 697.49	372,01	232,77	134.92 / 645.81
p-velocity saturated axial [m/s]	5254,63	299,79	4778.39 / 5478.26	4846,94	255,41	4362.88 / 5092.59	5007,56	155,97	4984.18 / 5053.60
p-velocity saturated radial [m/s]	5244,81	248,91	4634.83 / 5809.86	4833,65	168,93	4474.43 / 5238.10	4867,57	230,32	4591.84 / 5084.75
p-velocity dry axial [m/s]	5189,320	146,970	5031.95 / 5487.80	4776,150	102,940	4605.26 / 4910.71	4974,010	71,680	4876.16 / 5045.87
p-velocity dry radial [m/s]	5262,660	315,640	4910.71 / 5670.10	4732,210	213,330	4545.45 / 5015.20	4611,520	180,720	4375.87 / 4881.66
mean susceptibility [10-6 SI]	14620,00	1646,86	11910.00 / 17150.00	7254,5	993,88	6037.00 / 8665.00	11356,43	2863,64	7452.00 / 15730.00
NRM [A/m]	$7.22 \cdot 10^{-1}$	0.316	$9.85 \cdot 10^{-1}$ / 1.23	$3.60 \cdot 10^{-1}$	0.153	$4.06 \cdot 10^{-2}$ / $1.04 \cdot 10^{-1}$	$9.24 \cdot 10^{-1}$	0.358	$7.53 \cdot 10^{-1}$ / 1.39
lineation factor	1,008	0,003	1.005 / 1.013	1,018	0,006	1.007 / 1.028	1,010	0,003	1.006 / 1.014
foliation factor	1,016	0,006	1.009 / 1.024	1,007	0,001	1.014 / 1.037	1,011	0,003	1.015 / 1.037
degree of anisotropy	1,025	0,008	1.015 / 1.038	1,025	0,007	1.005 / 1.009	1,021	0,006	1.005 / 1.009

Table 3.2: Listing of the investigated petrophysical parameters of bulk density, grain density, porosity, electrical resistivity, compressional velocity, mean susceptibility, NRM and AMS measurement for fresh latite, latite and minor alterated lava. The table comprises the mean value, the respective standard deviation and the minimum and maximum value.

	alterated pseudo breccia			latitic lava			tuff		
	mean value	std deviation	min/max	mean value	std deviation	min/max	mean value	std deviation	min/max
bulk density [g/cm3]	2,460	0,060	2.37 / 2.51	2,300	0,080	2.12 / 2.43	2,070	0,040	2.03 / 2.13
grain density [g/cm3]	2,590	0,030	2.52 / 2.62	2,600	0,070	2.50 / 2.70	2,630	0,110	2.50 / 2.79
porosity [%]	5,120	1,660	4.14 / 8.54	11,620	2,810	7.36 / 17.63	21,250	3,220	16.57 / 25.91
electrical resistivity axial [Ωm]	214,62	96,18	79.45 / 295.34	119,87	99,81	34.65 / 370.87	30,11	9,72	18.70 / 38.13
electrical resistivity radial [Ωm]	286,99	118,09	182.26 / 452.01	127,08	85,15	52.90 / 297.57	36,86	10,37	24.65 / 51.57
p-velocity saturated axial [m/s]	4588,05	210,42	4291.55 / 4785.31	4160,28	203,25	3957.29 / 4280.16	3758,67	312,47	3405.41 / 4150.20
p-velocity saturated radial [m/s]	4676,61	178,28	4459.46 / 4896.14	4302,59	272,47	3810.62 / 4791.38	3800,60	161,69	3563.71 / 3997.68
p-velocity dry axial [m/s]	4576,020	179,260	43226.92 / 4741.38	3785,750	431,220	2853.26 / 4424.16	3076,100	530,300	2577.74 / 3810.62
p-velocity dry radial [m/s]	4719,870	71,820	4634.83 / 4810.50	4011,880	497,920	2837.84 / 4495.91	2984,690	20,770	2963.92 / 3005.46
mean susceptibility [10-6 SI]	1150,50	533,38	430.00 / 1703.00	1668,25	1379,73	350.00 / 4305.00	638,67	424,61	356.00 / 1373.00
NRM [A/m]	$1.31 \cdot 10^{-1}$	0.088	$7.31 \cdot 10^{-2}$ / $2.27 \cdot 10^{-1}$	$4.71 \cdot 10^{-1}$	0.353	$9.47 \cdot 10^{-2}$ / $1.27 \cdot 10^{-1}$	$1.53 \cdot 10^{-1}$	0.122	$4.03 \cdot 10^{-1}$ / $1.09 \cdot 10^{-1}$
lineation factor	1,010	0,006	1.005 / 1.019	1,014	0,014	1.002 / 1.046	1,004	0,003	1.002 / 1.010
foliation factor	1,014	0,009	1.009 / 1.034	1,011	0,007	1.006 / 1.059	1,005	0,004	1.005 / 1.019
degree of anisotropy	1,025	0,011	1.004 / 1.025	1,024	0,016	1.002 / 1.026	1,009	0,005	1.001 / 1.014

Table 3.3: Listing of the investigated petrophysical parameters of bulk density, grain density, porosity, electrical resistivity, compressional velocity, mean susceptibility, NRM and AMS measurement for alterated pseudo breccia, latitic lava and tuff. The table comprises the mean value, the respective standard deviation and the minimum and maximum value.

shield volcano is covered by sediments and the initial structure of the shield volcano should be faultless.

In the course of a study performed by the Geological Survey of Austria the drill core was described and investigated in terms of mineralogy, chemistry and susceptibility. Furthermore, a core profile distinguishing the various layers and lithologies was derived. Based on this investigation the samples used within the present study were classified in terms of rock type and thus, the petrophysical parameters of the lithologies of fresh latite, minor alterated lava, latite, alterated pseudo breccia, latitic lava and tuff were derived (tab. 3.1). The petrophysical parameters obtained are expected to differentiate the various lithologies observed and reflect the layered structure. Moreover, the anisotropy of the rocks is assumed to yield to further characterization possibilities.

Starting with the analysis of the parameters bulk density and porosity a first differentiation of the various lithologies is possible (fig. 3.5a). The rock types show a decrease in bulk density as the porosity values increase. Fresh latite is indicated by the highest bulk density and the lowest porosity whereas tuff shows contrary features with the lowest bulk density and the highest porosity values. The sequence within these end-members is latite, minor alterated lava, alterated pseudo breccia and latitic lava. The same trend in correlation with porosity as well as the lithology sequence is given in the cross plots of grain density, electrical resistivity, mean susceptibility and p-velocity (fig. 3.5b, 3.6, 3.8a and 3.10a, b). In terms of the NRM measurement versus mean susceptibility an overall positive correlation is observed although the results for the NRM measurements scatter (3.8b).

The analysis of the investigated parameters allows a clear distinction of the lithologies involved. The sequence of lithology described shows a distinction concerning mean susceptibility (fig. 3.13) and moreover, an affinity of different lithologies is recognizable. Fresh latite, latite and minor alterated lava likely emanate from the same lava type with a specific composition. The difference of these three rock types are minor and are affected by the circulation of hydrothermal water after the formation process and weathering effects. Considering the lithologies latitic lava and alterated pseudo breccia, Belocky et. al. (1996) describe the second lithology as derivate of latitic lava. Thus, the alteration processes caused a chemical modification which leads to lower values in porosity and increases the petrophysical features of bulk density, electrical resistivity, mean susceptibility and p-velocity. The last rock type involved, tuff, shows a clear distinction from all other lithologies which is affected by the history of origin. The survey of the parameters grain density versus porosity shows outliers within this

group which are ascribed to large, newly formed carbonatic crystals after the influence of hydrothermal alteration processes (Belocky et. al., 1996).

In order to enable a further characterization of the internal structure of the lithologies the anisotropy was investigated by means of axial and radial measurements in terms of electrical resistivity and p-velocity. The results show variations in the directional measurements indicating a significant anisotropy degree for most samples (fig. 3.7, 3.11 and 3.11). Investigating the results for each lithology no preferred anisotropy direction, along the axial or radial axis, is observed. The AMS measurement used to characterize the ellipsoidal shape of the fabric shows scattering results and the values are small ($\leqslant 1.05$). The degree of anisotropy obtained by means of the AMS measurement shows a wide range of values within each lithology (fig. 3.9a) and there is no correlation of a specific degree of anisotropy to a rock type obvious (fig. 3.13b). Thus, the analysis of the coefficient of anisotropy and the degree of anisotropy is uncertain.

In terms of lineation factor versus foliation factor the same overall scattering trend is valid (fig. 3.9b). There are only two lithologies which are indicated by one shape type, fresh latite plots within the oblate shape and latite within the prolate shape. The oblate shape is likely affected by the load of the volcano as this lithology occurs at depth levels of 705m and 762m. As latite is in all its features similar to fresh latite an oblate shape would be assumed. Latite occurs at depth levels of 651m and 654m and, as stated above, a derivate of fresh latite. The influence of weathering processes and the circulation of hydrothermal fluids caused the modification of the magnetization carrier and its crystal shape. This mutation is most likely observed in the difference in ellipsoidal shape.

The structure of the shield volcano, i.e. single layers, as described in Belocky et. al (1996) is difficult to differentiate in terms of petrophysics. As the samples within this investigation are taken every 50m, a continuous observation is not possible and therefore a detailed profile can not be constructed. A comparison of all observed parameters versus depth is given in fig. 3.15. The only parameter allowing a differentiation in terms of layers is mean susceptibility. Although layers are obvious, a distinction of latitic lava and alterated pseudo breccia is not seen as the mean susceptibility of the lithology varies in nearly the same range. Hence, the boundary between the two rock types is overlooked. However, between the depth levels of 651m and 762m an increasing trend of all surveyed parameters is observed. Considering tab. 3.1 latite and fresh latite occur in this section. The variation of the results are connected to alteration processes caused by hydrothermal fluids as the lithologies show affinity as stated earlier.

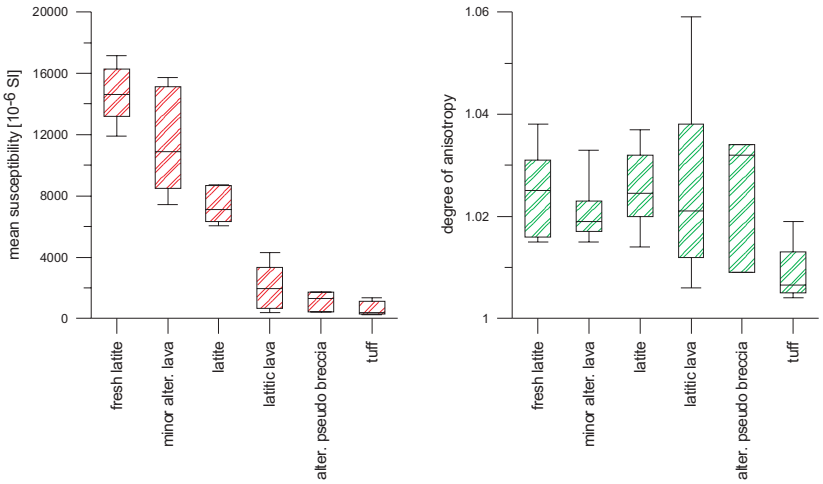

Figure 3.13: Box plot of mean susceptibility and anisotropy degree. A decrease in mean susceptibility from fresh latite, minor alterated lava, latite, latitic lava, alterated pseudo breccia and tuff is observed. The analysis of the degree of anisotropy shows results within the same range for the lithologies available.

Hence, the petrophysical parameters reflect the alteration and weathering processes occurring to the rocks. From depth level 345m to 501m a decreasing trend is observed which indicates the alteration process from latitic lava towards minor alterated lava. The decrease in porosity, bulk density, resistivity and p-velocity is affected by the mineralization of new crystal due to the circulation of hydrothermal fluids within the formation (Belocky et. al., 1996). Thus, the latitic lava located at the lower depth level (501m) is minor influenced by the weathering effect.

Cross plots of the anisotropy degree obtained for the magnetic measurement, electrical resistivity and p-velocity in dry and saturated condition are plotted in fig. 3.14. In terms of anisotropy degree of magnetic measurement and p-velocity obtained in saturated condition a positive correlation is observed (fig. 3.14c). An increasing degree of magnetic anisotropy results in an increase of the anisotropy degree for p-velocity obtained in saturated condition. The magnetic anisotropy degree is lower than the degree of anisotropy for p-velocity (saturated). The correlation of the anisotropy degrees is eye-catching, but a grouping of the lithologies as determined in terms of absolute values is not detected. The same trend, although not that striking, occurs within the cross plot of magnetic anisotropy degree versus degree of anisotropy for p-velocity measured in dry condition. In terms of degree of anisotropy of electrical resistivity versus degree of magnetic anisotropy no correlation is found.

Considering these results the comparison of absolute values allows a differentiation

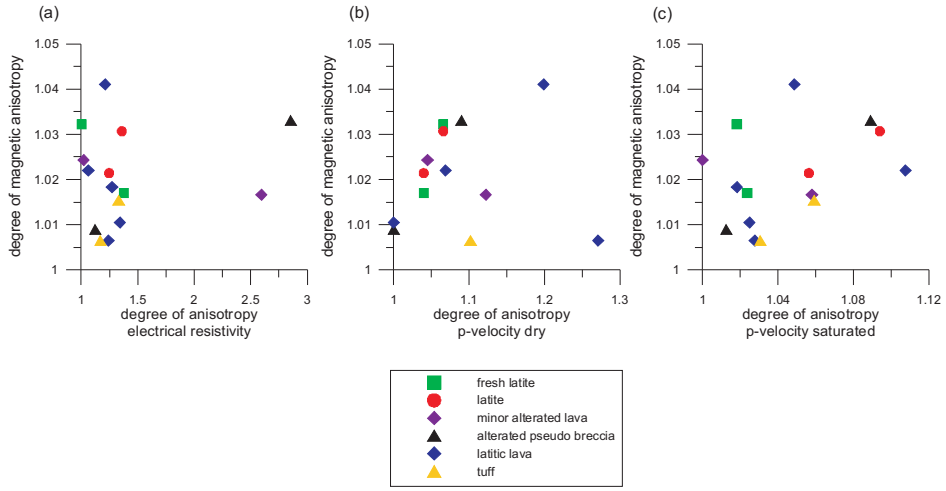

Figure 3.14: (a) Plot of the degree of magnetic anisotropy versus the degree of anisotropy of electrical resistivity. The results for the magnetic anisotropy degree vary whereas the degree of anisotropy of electrical resistivity is located around 1.25; (b) Plot of the degree of magnetic anisotropy versus the degree of anisotropy of p-velocity measured in dry condition. A positive correlation between the two parameters with increasing values is observed; (c) Plot of the magnetic anisotropy degree versus the degree of anisotropy of p-velocity obtained in saturated condition. With increasing magnetic anisotropy degree the anisotropy degree of p-velocity (saturated condition) increases.

of the lithologies involved whereas the correlation of magnetic and p-velocity anisotropy degree indicates a connection of the two parameters, but a characterization of various lithologies is uncertain.

In conclusion it can be stated that the petrophysical measurement methods obtain good results for the distinction of the various lithologies involved. The characterization of the layered structure of the shield volcano is difficult as the layers change rapidly (Belocky et. al, 1996) and the sampling did not cover all lithologies available. However, a tracking of alteration processes after investigating the lithological features is possible. Considering the investigation in terms of anisotropy a further characterization is difficult as the coefficient of anisotropy calculated for the electrical, elastical and magnetic measurements do not allow a correlation to a single lithology. The results obtained by means of the AMS measurement are very small ($\leqslant 1.05$) although significant. Due to the small values the results for the degree of anisotropy and the lineation and foliation factor scatter and no preferred shape, e.g. oblate or prolate, can be determined. As the shield volcano of Bad Gleichenberg was not part of a destructive event after its forming process the unoriented structure is plausible.

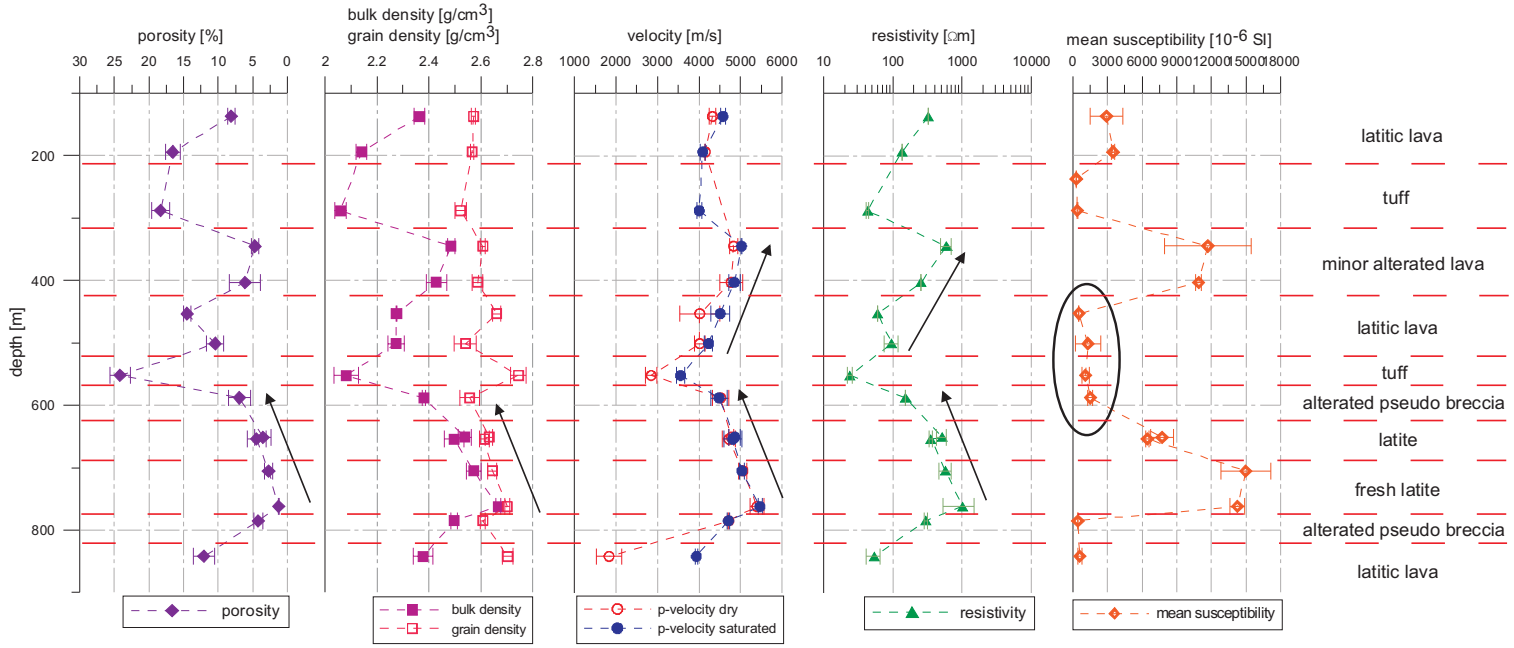

Figure 3.15: Plot of all investigated parameters observed versus depth in comparison. From left to right occur porosity, bulk density and grain density, p-velocity measured in dry and saturated condition, electrical resistivity and mean susceptibility. A description of the core in terms of lithology is given at the right side. A significant differentiation of the layered volcanic structure is difficult, but alteration trends (black arrows) are observed after a detailed petrophysical description of the involved lithologies between the depth levels of 345m and 501m as well as between 651m and 762m. The only parameter indicating a layered structure is mean susceptibility, but this parameter shows no difference between alterated pseudo breccia and latitic lava (oval drawing) and therefore restrictions have to be set.

Chapter 4

Böhmische Masse

4.1 Geology

The Bohemian Massif of Austria is located in the northern federal states of Upper and Lower Austria (fig. 4.1). As part of the Variscian mountain chain which was formed in the Paleozoic starting in the Ordovician Periode (542 mya), the Austrian part of the Bohemian Massif forms the eastern tail of the orogen (fig. 4.2) (Tollmann, 1985). The two representatives within Austria are the Moravian and Moldanubian unit which are separated by the Moldanubian thrust fault. The Moravian unit located east to the Moldanubian thrust fault is subducted under the Moldanubian unit. The Moldanubian unit located west to the thrust fault and representing the larger unit spreads out to the Black Forest of Germany, large parts of France as the Armorican Massif of Brittany and Normandy, the Massif Central and the Vosges as well as the Iberian Peninsula (fig. 4.2) (Tollmann, 1985). In consequence of the subduction melting processes occurred which forced the late variscian intrusion of the South Bohemian Pluton into the Moldanubian unit (Tollmann, 1985) which hence is seen as the third major unit within the Bohemian Massif of Bavaria, Czech Republic and Austria (Ebner, 1997).

The Variscides have been a high mountain chain but due to erosion the only remainder of the Variscides in Austria is the crystalline basement of the Bohemian Massif with its complex nappe pile (Tollmann, 1985). Subsequent a first overview on the complex nappe pile is given (Tollmann, 1985):

A Moravian unit (deepest unit)

B Moldanubian unit

1. Drosendorf unit

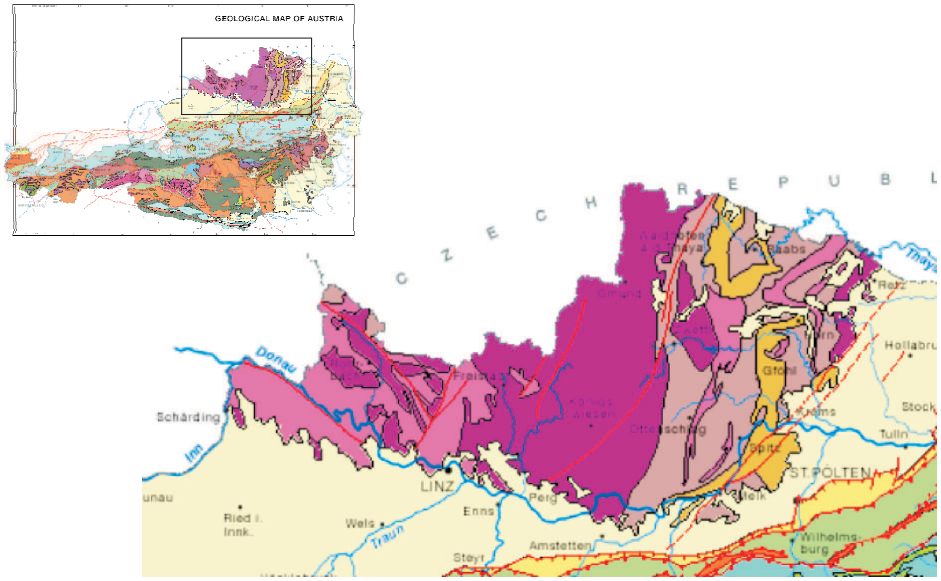

Figure 4.1: Location of the Austrian part of the Bohemian Massif in the federal states of Upper and Lower Austria (Geologische Bundesanstalt, 2006).

a Ostrong unit

b Mühldorf unit

2. Gföhl unit

a Raabs–Meisling unit

b Gföhl gneiss unit

c St. Leonhard unit

C Barrandian unit (shallowest unit)

The lithologies evident in the Moravian and Moldanubian unit are both crystalline but they can be distinguished as the Moravian unit shows a low degree metamorphism whereas the Moldanubian unit is indicated by a high degree metamorphism (Tollmann, 1985).

The Moravian unit east to the Moldanubian thrust fault subducts under the Moldanubian unit and is seen as its basement (Tollmann, 1985). It consists of a nappe pile with three units, the Thaya batholith as the bottom unit which is overlied by the Pleissing nappe and finally the Bittesch gneiss nappe lies on top (Friedl et. al, 2004). The Thaya batholith is formed by intruded granite, granodiorite, tonalite and diorite rock types with an age of 551 ± 6mya (Tollmann, 1985). The Pleissing nappe consists of two lithologies whereas the Weitersdorf Stengel gneiss with its high schistosity forms the

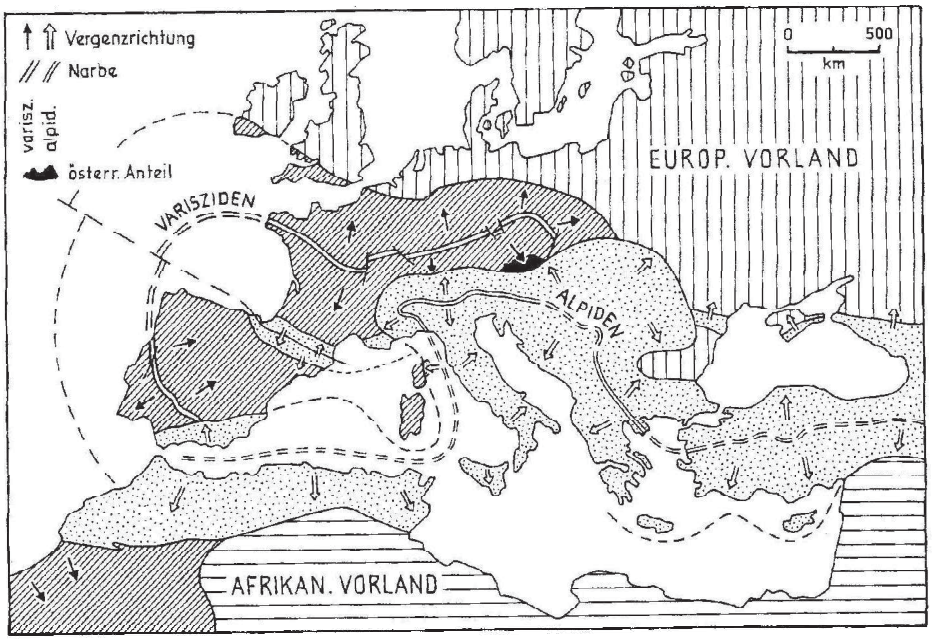

Figure 4.2: The location of the Variscian mountain chain within Europe and the position of the Austrian part after A. Tollmann in Tollmann (1985)

bottom lithology and the mica slate marble series the top lithology (Tollmann, 1985). The top nappe, Bittesch gneiss nappe, consists of a strongly deformed orthogneiss (Friedl et. al, 2004).

The Moldanubian unit has to be characterized separately for the parts in Lower and Upper Austria as the unit is cut into pieces due to the intrusion of the South Bohemian Pluton.

The units occurring in Lower Austria show a complex nappe pile from bottom to top consisting of the Monotonous series, layers of granulite, Dobra Gneiss, Variegated series, Raabser series, Gföhler gneiss and granulite. A peculiarity of this unit is the top position of the high degree metamorphism rocks whereas the low degree metamorphism rocks are located at the bottom (Tollmann, 1985).

In Upper Austria the Moldanubian unit is divided into three zones due to late Variscian shear zone systems (fig. 4.3)(Ebner, 1997). The two major faults, the Bavarian Pfahl and the Danube fault, are dextral shear zones which were formed in the very late Variscian age after the major granite intrusions around 294 ± 8mya with ductile deformation processes at a high temperature level (Wallbrecher et al., 1993). North of the Bavarian Pfahl the Bohemian forest zone characterized by schistous gneiss occurs (Ebner, 1997). South of the Bavarian Pfahl the Mühl zone with the lithologies of

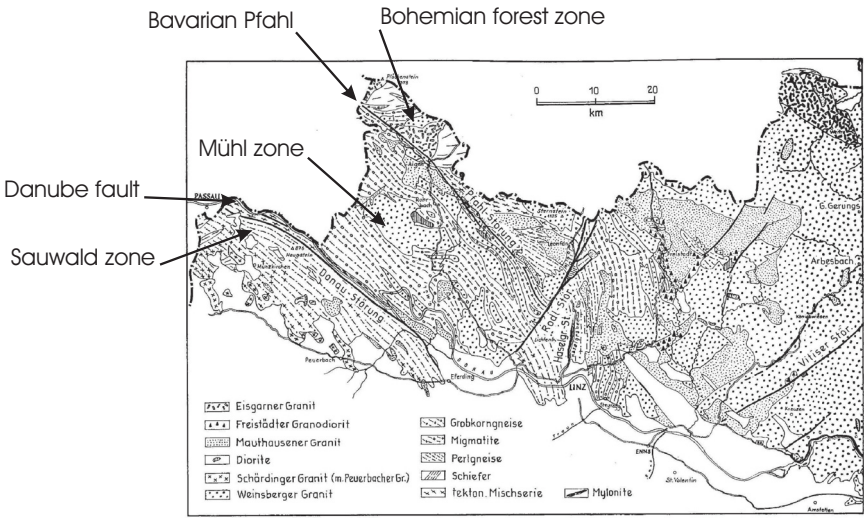

Figure 4.3: Simplified drawing of the Moldanubian unit in Upper Austria after o. Thiele and G. Fuchs & A. Matura in Tollmann (1985) indicating the Bavarian Pfahl and Danube fault as well as the Bohemian forest zone, Mühl zone and Sauwald zone.

Weinsberg granite and coarse-grained granite appears (Ebner, 1997). In the south the Mühl zone is bordered by the Danube fault (Ebner, 1997). South of the Danube fault the Sauwald zone occurs with Schärding granite as major rock type (Tollmann, 1985).

A major part of the Austrian Bohemian Massif is formed by the South Bohemian Pluton which intruded after melting processes occurring due to the subduction of the Moravian unit under the Moldanubian unit (Friedl et. al, 2004). Hence a variety of granites intruded into the Bohemian Massif in the late Variscian orogeny. The South Bohemian Pluton occurs westward along the line of Ispertal–Gutenbrunn–Zwettel–Zlabings and comprises the western part of the Waldviertel and the eastern part of the Mühlviertel to the meridian of Linz (Ebner, 1997). Among the intrusions to the west of the Mühlviertel and Sauwald parts of the crystalline basement are still present (Ebner, 1997). The South Bohemian Pluton with its intrusions spreads out along Perg, Gmünd, Litschau until westward of Iglau in the Bohemian–Moravian borderland (Tollmann, 1985).

Due to varying cooling times and mineral composition a chronology of the intrusion can be given by means of the various types of granite. The oldest lithology occurring is the Rastenberg granite with its cooling period in the carboniferous age (359–299 mya). Subsequent the Weinsberg granite within the Mühl zone follows and after this the Schärding granite located in the Sauwald zone is formed. Following this the Mau-

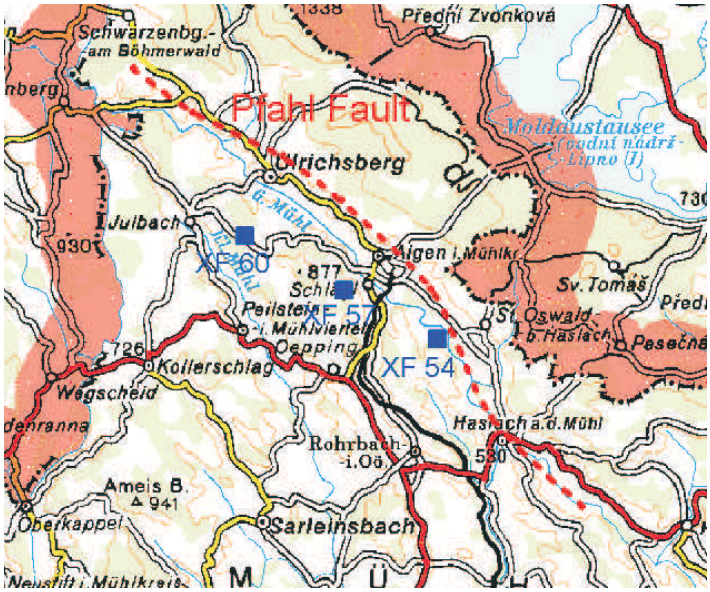

Figure 4.4: Section of Upper Austria indicating the Bavarian Pfahl and the sample locations XF54 (∼0.16km), XF57 (∼1.28km) and XF60 (∼2.79km).

thausen granite intrudes in the already existing Weinsberg granite unit especially between Leonfelden and Aigen. The age of the Mauthausen granite is dated 304 ± 6mya but due to reheating process the age is too young to be the real forming age. The last granite type is called Eisgarn granite and is located in the north of Lower Austria. In addition to the intrusions described above the South Bohemian Pluton formed dykes which are mainly located next to Persenbeug, Loja–valley, Raabs and Waidhofen (Tollmann, 1985).

The specimens used within in this survey are located in the Mühl zone with varying distances to the Bavarian Pfahl (fig. 4.4). The picked samples are fine grained granites where sample location XF54 and XF57 are of Schlägel granite type and sample location XF60 is of Weinsberg granite tending to Schlägel granite type (tab. 4.1).

4.2 Results

The samples of the Bohemian Massif investigated within this survey were collected in course of a scientific project (project S47–07) financed by the Austrian Research Foundation (FWF) in the 1990s. The cylindrical shaped samples were drilled oriented in quarries and roadcuts and have a diameter of $25mm$ and a length of $\backsim 20mm$. For the present study three locations were selected varying in the distance to the center of the Bavarian Pfahl (fig. 4.4). The total amount of plugs investigated is 29 and all

sample ID	lithology	distance to Bavarian Pfahl [km]	total number of samples
XF54	Schlägel granite	~ 0.16	11
XF57	Schlägel granite	~ 1.28	6
XF60	Weinsberg granite/Schlägel granite	~ 2.79	12
$\sum$			**29**

Table 4.1: Listing of sample ID, lithology specification, distance to the Bavarian Pfahl and total number of samples investigated referring to the sample locations.

measurement methods were applied to the total number of samples.

4.2.1 Density and Porosity

The bulk density, grain density and porosity data obtained applying the Archimedes' Principle are plotted in fig. 4.5.

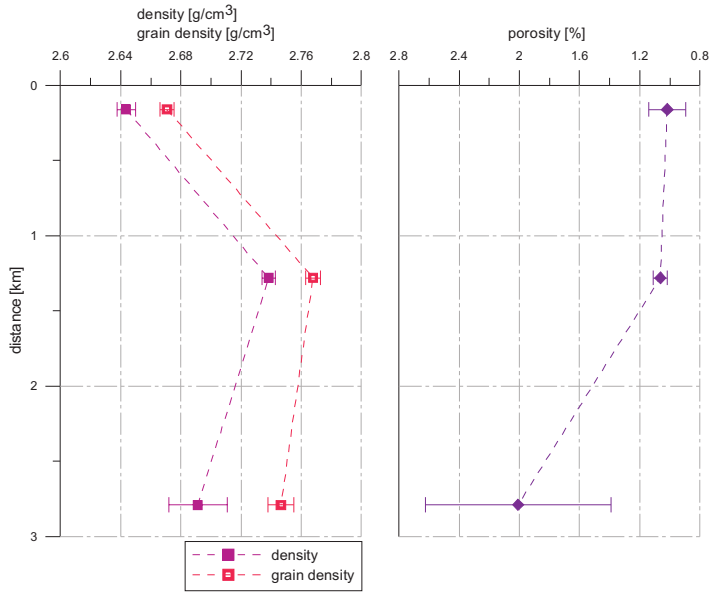

Figure 4.5: Plot of the results of bulk density, grain density and porosity versus distance in km to the Bavarian Pfahl; bulk density and grain density in g/cm^3 show an increase towards location XF57 and a decrease towards location XF60; porosity in % increases with increasing distance to the Bavarian Pfahl.

The bulk density varies in the range of 2.64 to 2.74 g/cm^3 with a standard deviation of $\pm 0.37\%$. The sample location XF54 next to the Bavarian Pfahl has a bulk density

value of 2.64 g/cm^3. Sample location XF57 shows an increase in bulk density which is followed by a decrease measured at the farthest sample location XF60.

In view of grain density the values vary in the range of 2.67 to 2.77 g/cm^3 with a standard deviation of ±0.22%. The trend given by the bulk density data is also observed in terms of grain density (fig. 4.5).

The porosity data vary in the range of 1.02 to 2.01 % (fig. 4.5). The standard deviation is ±19.2% and was calculated for each porosity value to be 100%. Sample location XF54 has the lowest porosity value with 1.02%. Starting from this point an increase to sample location XF60 with a porosity value of 2.01% occurs.

4.2.2 Electrical properties

The electrical properties are observed measuring the electrical resistivity in axial and radial direction. The results plotted in fig. 4.6 show the variation of the average electrical resistivity in axial and radial direction with increasing distance to the Bavarian Pfahl. Furthermore the coefficient of anisotropy is drawn illustrating the structural change.

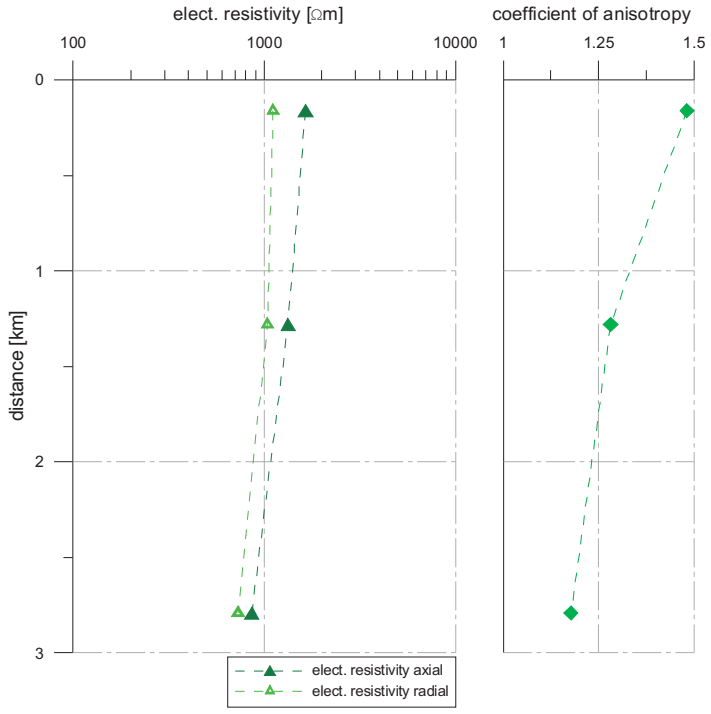

Figure 4.6: Plot of the average electrical resistivity values in axial and radial direction and the coefficient of anisotropy versus distance to the Bavarian Pfahl; both diagrams show a decreasing trend with increasing distance to the Bavarian Pfahl.

The average electrical resistivity results vary in the range of 857 to 1645 Ωm in axial direction and 728 to 1111 Ωm in radial direction. The accuracy of the measurement method is given by $\pm 1\%$ due to additional measurements. Analyzing the average values of electrical resistivity in axial direction a steady decrease from sample location XF54 ($\sim$0.16km) till sample location XF60 ($\sim$2.79km) occurs. The same trend but with lower values for the electrical resistivity is observed investigating the results in radial direction (fig. 4.6).

Subsequent to this analysis the ratio between axial and radial direction, the coefficient of anisotropy, was calculated (fig. 4.6). Considering that a value of 1.00 for the coefficient of anisotropy indicates isotropy the sample locations show a decrease in terms of anisotropy with increasing distance to the Bavarian Pfahl. Moreover the anisotropy is characterized by higher values in resistivity in axial direction for all three sample locations.

4.2.3 Magnetic properties

The magnetic properties of the samples were determined by measuring the anisotropy of the magnetic susceptibility (AMS) and the natural remanent magnetization (NRM) with succeeding AF–demagnetization.

The mean magnetic susceptibility plotted in fig. 4.7 determined by means of a Kappabridge KLY–2 varies in the range of 132 to $424 \cdot 10^{-}6SI$ with a standard deviation of $\pm 11.5\%$. At sample location XF54 the lowest mean susceptibility value, $132.00 \cdot 10^{-}6SI$, is observed. Starting from this sample location a continuous increase to the farthest sample location XF60, with a mean susceptibility of $424.24 \cdot 10^{-}6SI$, is observed.

The plot NRM versus mean susceptibility shows a positive correlation between the two parameters (fig. 4.8a). Hence an increase in NRM shows an increase in mean susceptibility. Three groups correlative to the sample locations occur, with sample location XF54 next to the Bavarian Pfahl yielding the lowest mean susceptibility and NRM values.

The cross plot of mean susceptibility versus degree of anisotropy shows a decreasing degree of anisotropy with increasing mean susceptibility values (fig. 4.8b). Hence sample location XF54 is characterized by the lowest mean susceptibility values and the highest anisotropy degree by contrast to sample location XF60 indicated by the highest mean susceptibility values and the lowest degree of anisotropy. Nevertheless the groups detected in fig. 4.8a can also be observed within this plot.

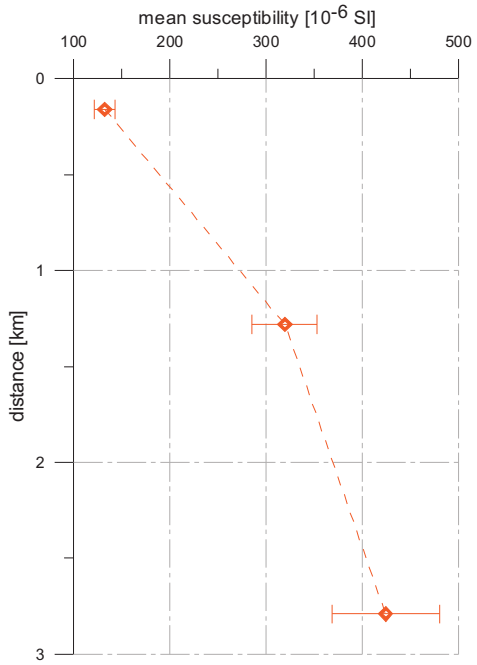

Figure 4.7: Plot of the mean magnetic susceptibility [$10^{-}6SI$] versus distance [km]. Starting at sample location XF54 a continuous increase towards the farthest sample location XF60 occurs.

Plotting foliation factor versus lineation factor a first analysis of the ellipsoidal shape of the magnetic particles is possible (fig. 4.8c). The diagram is separated into two halves by a solid line which indicates the zone of triaxial shape and furthermore acts as borderline between the zones of prolate and oblate shape. The samples of location XF54 show a prolate shape. The overall shape of sample location XF57 and XF60 is oblate. Although the locations XF57 and XF60 show an oblate shape two distinct groups are observable as sample location XF60 leans towards triaxial shape (fig. 4.8c).

The results of the NRM and succeeding AF–demagnetization measurements are presented in fig. 4.9. Sample location XF54 has a low NRM value with $1.44 \cdot 10^{-4} A/m$ and subsequent the AF–demagnetization process is short and ends at 13mT (fig. 4.9a). The curve follows a continuous decrease to its end AF–demagnetization value with a median destructive field of 8mT. The demagnetization curve of sample location XF57 has a NRM value of $1.43 \cdot 10^{-3} A/m$ (fig. 4.9b). The demagnetization process results in an enhancement of the existing magnetization and therefore the demagnetization process was aborted at 20mT. The median destructive field was not met. The farthest sample location XF60 with a NRM value of $1.52 \cdot 10^{-5} A/m$ shows a sudden decrease

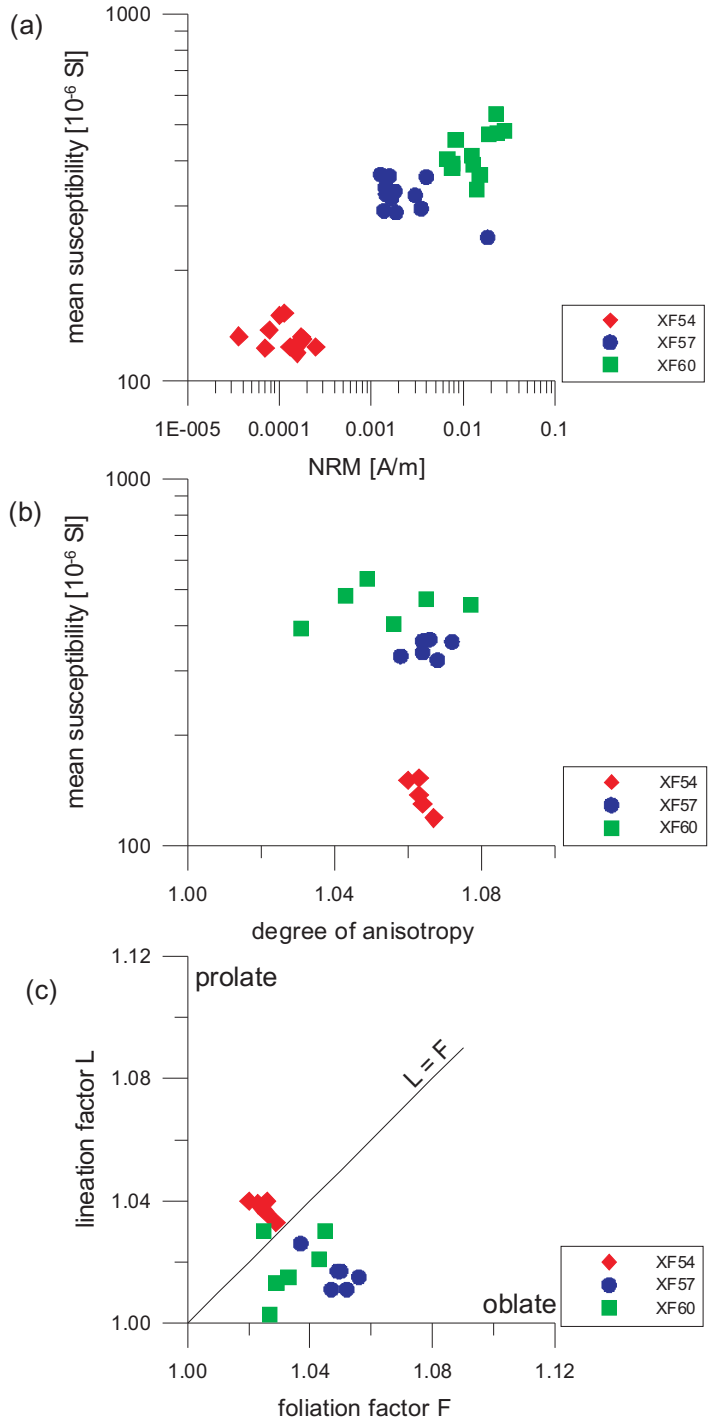

Figure 4.8: (a) Plot of mean magnetic susceptibility [$10^{-}6SI$] versus NRM [A/m] showing that increasing mean susceptibility values correlate with increasing NRM values; (b) Cross plot of mean magnetic susceptibility versus degree of anisotropy. The degree of anisotropy decreases with increasing magnetic susceptibility; (c) Plot of foliation factor versus lineation factor. The solid line indicates the zone of triaxial shape and furthermore the boundary between prolate and oblate shape.

in demagnetization and ends at the 100mT-step (fig. 4.9c). The median destructive field is at 10mT.

4.2.4 Elastic properties

The velocity data were obtained applying an ultrasonic transit–time measurement method to obtain compressional velocities of the investigated samples. The measurement equipment allows an accuracy for the offset–time of $0.04\mu s$ as this is the smallest measurement grid. In order to obtain a broad data set the samples were measured in dry and saturated condition in axial and radial direction.

The samples measured in saturated condition in axial direction have velocity values in the range of 4990 to 6038 m/s with a standard deviation of $\pm 5.47\%$ (fig. 4.10). For the velocity determination along the radial axis results in the range of 4911 to 5546 m/s with a standard deviation of $\pm 1.70\%$ were obtained. The course of the curve with increasing distance to the Bavarian Pfahl shows a slight increase between sample location XF54 and XF57 and a decreasing trend between XF57 and XF60. The described course of the curve matches the results measured along the axial and radial axis with the exception that the results in radial direction are lower than in axial direction. Analysing the ratio between axial and radial direction, the coefficient of anisotropy shows the same trend as described for the course of the compressional velocity results (fig. 4.10).

The compressional velocities measured on dry samples in axial direction vary in the range of 4288 to 5355 m/s with a standard deviation of $\pm 2.88\%$ (fig. 4.11). Sample location XF54 has a p-velocity value of 5355.46 m/s which is followed by a slight increase to sample location XF57. After this a rapid decrease to the farthest sample location XF60 occurs indicated by the lowest p-velocity value observed. The p-velocity results measured in dry condition along the radial axis vary between 3849 and 5033 m/s with a standard deviation of $\pm 2.26\%$. Although the results obtained in radial direction are lower than in axial direction, the overall trend as described in axial direction is also recognizable (fig. 4.11). The analysis of the coefficient of anisotropy shows a continuously increasing trend from sample location XF54 to XF60 (fig. 4.11).

Comparing the results obtained measuring the samples in dry and saturated condition in axial and radial direction a good conformity is obvious. Only the coefficient of anisotropy measured in dry condition shows a contrary trend to the result obtained by the saturated condition measurement.

A summary of all investigated petrophysical parameters indicated by means of a

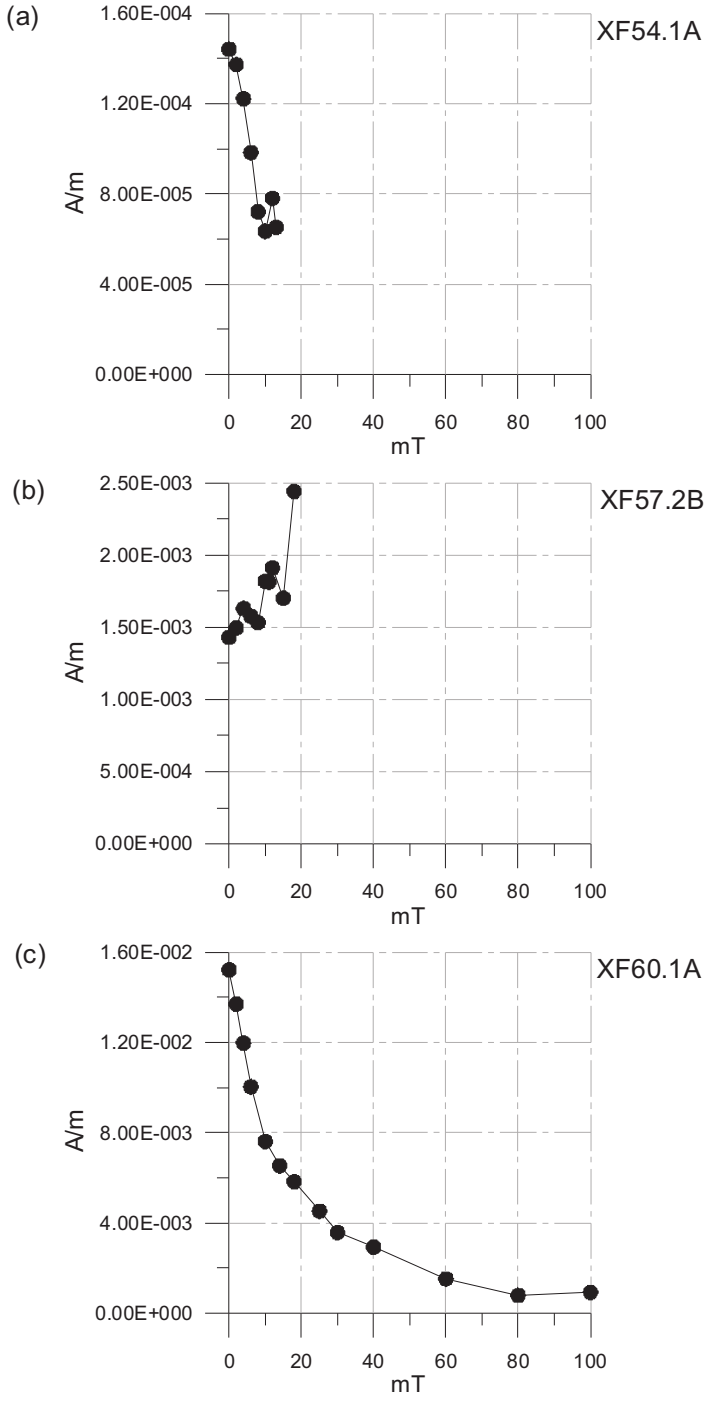

Figure 4.9: Plot of the AF–demagnetization curve in [mT] versus the remaining magnetization J [A/m] for location XF54 (a), XF57 (b) and XF60 (c); The median destructive field was only met by sample location XF54 (8 mT) and XF60 (10 mT) as sample location XF57 shows an enhancement in magnetization.

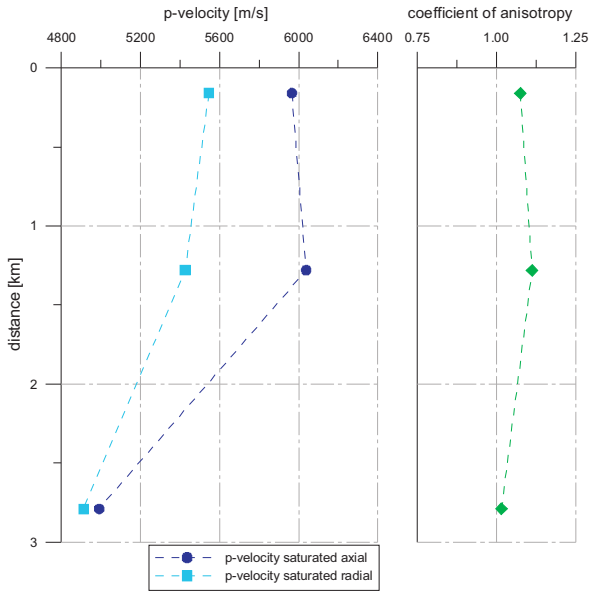

Figure 4.10: Plot of the compressional velocities in axial and radial direction measured in saturated condition and the anisotropy coefficient versus distance [km]. The results of the axial measurement show higher values in contrast to the results obtained along the radial axis.

numerical presentation is given in tab. 4.2 by the mean value, the respective standard deviation and the minimum and maximum value.

4.3 Discussion

The Bohemian Massif of Austria is mainly influenced by the intrusion of the South Bohemian Pluton and the afterwards installed fault systems, the Bavarian Pfahl or Danube fault (Friedl et. al, 2004). The fault systems are characterized by ductile deformation processes in a high temperature range (Wallbrecher et al., 1990). The samples of this survey were taken from intrusions of the South Bohemian Pluton in varying distances to the Bavarian Pfahl within the Mühl zone (fig. 4.4). The surveyed types of granite, Schlägel granite, are comparable in terms of mineralogy and texture. Hence, the investigation of petrophysical parameters and their directionality with increasing distance to the Bavarian Pfahl should allow a distinction of the sample locations.

In fig. 4.12 the petrophysical parameters versus distance are plotted. Eye-catching is the decreasing trend for porosity, electrical resistivity and compressional velocity measured in dry and saturated condition with increasing distance to the Bavarian Pfahl.

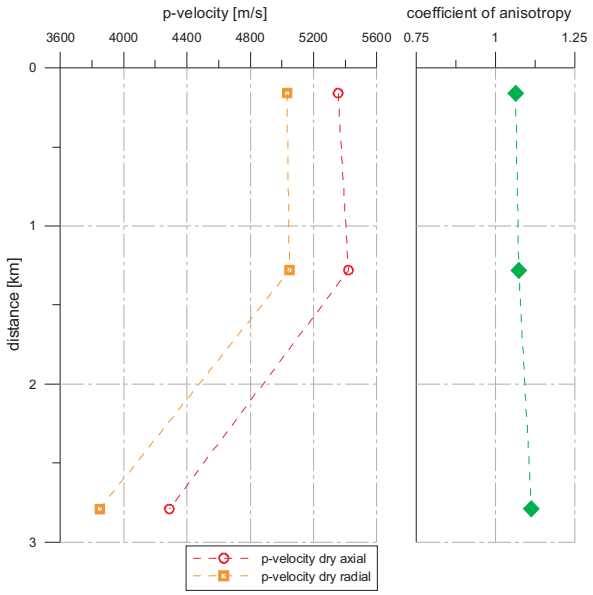

Figure 4.11: Plot of the compressional velocities in axial and radial direction obtained measuring the samples in dry condition and the coefficient of anisotropy versus distance [km]. The results of the axial measurement show higher values as the radial measurement results.

The mean susceptibility shows a contrary trend as the values increase with increasing distance. The magnetization carrier characterized during the AF–demagnetization process is magnetite which varies in concentration from one sample location to the other. However, a first overview on the surveyed properties allows a distinction of the three sample locations.

Starting at sample location XF54 next to the Bavarian Pfahl a significant change to sample location XF57 can be seen analyzing the bulk density and grain density data (fig. 4.12). At sample location XF54 the bulk density has a value of 2.64 g/cm^3 which increases until location XF57 to a value of 2.74 g/cm^3. The same is valid in terms of grain density (fig. 4.12).

The cross plot of mean susceptibility and NRM shows two distinct groups for the sample locations. The mean susceptibility as well as the NRM is low at sample location XF54 and increases significantly at sample location XF57 (fig. 4.8a). The AF-demagnetization process characterizes the magnetization carrier as magnetite. In case of sample location XF54 the magnetite concentration is low. The AF–demagnetization curve obtained for location XF57 is unfortunately an outlier which can also be seen in other diagrams. However, the positive correlation between mean susceptibility and NRM indicates the result.

An increasing trend of the values occurs in terms of mean susceptibility as well as

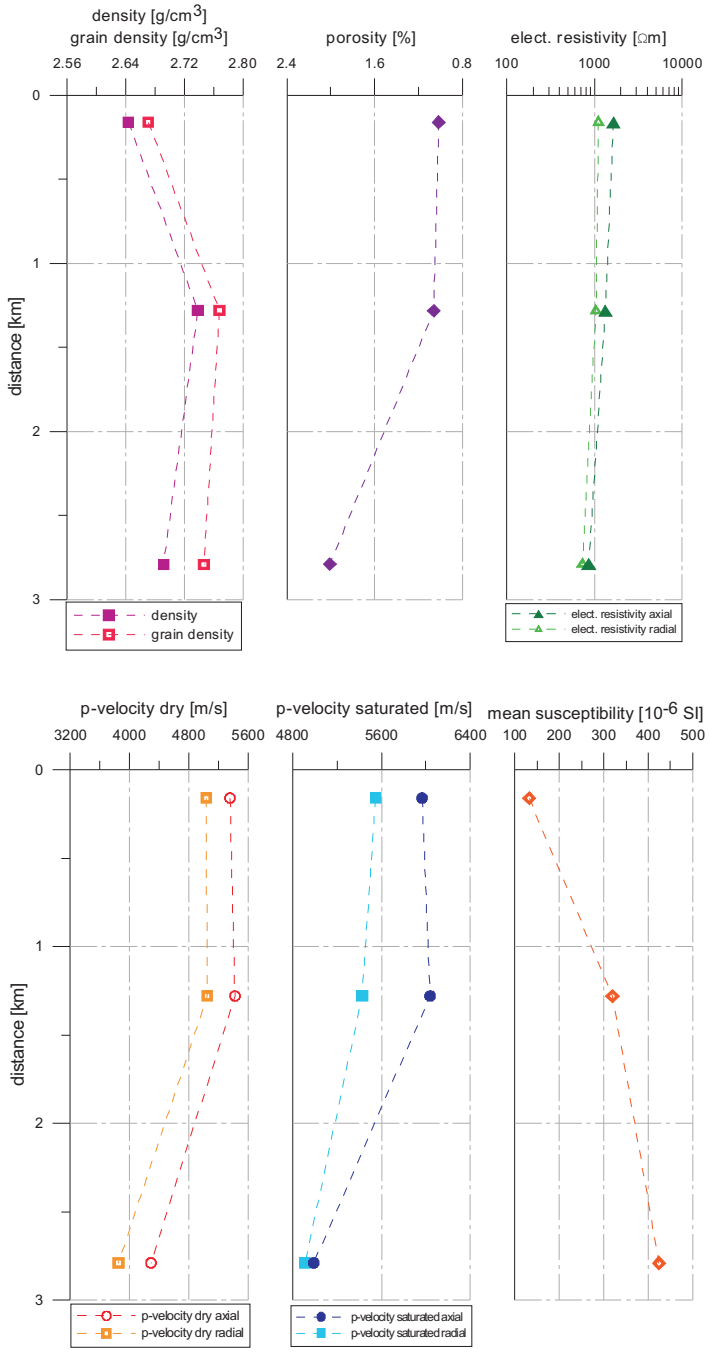

Figure 4.12: Compilation of all investigated parameters, bulk density, grain density, porosity, electrical resistivity, compressional velocity in dry and saturated condition and mean susceptibility versus distance. The course of the curves allows a distinction between the sample locations observed.

	XF54			XF57			XF60		
	mean value	std deviation	min/max	mean value	std deviation	min/max	mean value	std deviation	min/max
bulk density [g/cm3]	2,640	0,006	2.63 / 2.65	2,740	0,005	2.73 / 2.74	2,690	0,019	2.64 / 2.70
grain density [g/cm3]	2,670	0,004	2.66 / 2.68	2,770	0,005	2.76 / 2.77	2,750	0,009	2.73 / 2.76
porosity [%]	1,020	0,122	0.70 / 1.14	1,060	0,047	0.97 / 1.12	2,010	0,016	1.27 / 3.80
electrical resistivity axial [Ωm]	1644,11	136,82	1433.74 / 1838.03	1329,93	249,53	887.39 / 1594.37	857,55	178,56	651.50 / 1586.95
electrical resistivity radial [Ωm]	1110,24	317,58	791.29 / 1907.46	1038,17	264,21	770.89 / 1392.78	728,37	106,75	549.34 / 930.25
p-velocity saturated axial [m/s]	5965,52	89,39	5397.40 / 5746.15	6037,61	30,15	5381.84 / 5468.52	4990,80	151,18	4686.32 / 5116.44
p-velocity saturated radial [m/s]	5545,44	376,26	5351.49 / 6604.70	5425,79	147,29	5762.71 / 6226.42	4911,50	405,25	4350.00 / 5557.55
p-velocity dry axial [m/s]	5335,460	132,040	5163.51 / 5647.67	5420,730	117,840	5312.50 / 5596.25	4288,370	184,060	4011.83 / 4518.57
p-velocity dry radial [m/s]	5032,080	74,910	4940.48 / 5216.48	5048,120	65,010	4993.32 / 5173.13	3849,030	175,160	3516.95 / 4104.40
mean susceptibility [10-6 SI]	132,00	10,95	119.30 / 153.50	319,36	17,47	321.00 / 365.60	424,24	55,95	333.60 / 533.90
NRM [A/m]	$1.26 \cdot 10^{-4}$	$5.71 \cdot 10^{-5}$	$7.84 \cdot 10^{-5}$ / $1.19 \cdot 10^{-4}$	$2.18 \cdot 10^{-3}$	$9.88 \cdot 10^{-4}$	$3.99 \cdot 10^{-3}$ / $1.27 \cdot 10^{-3}$	$1.55 \cdot 10^{-2}$	$6.82 \cdot 10^{-3}$	$8.29 \cdot 10^{-3}$ / $1.25 \cdot 10^{-2}$
lineation factor	1,038	0,003	1.033 / 1.040	1,016	0,005	1.011 / 1.026	1,019	0,010	1.003 / 1.030
foliation factor	1,025	0,003	1.023 / 1.029	1,049	0,006	1.037 / 1.052	1,034	0,008	1.025 / 1.045
degree of anisotropy	1,063	0,002	1.060 / 1.067	1,065	0,004	1.058 / 1.072	1,054	0,015	1.031 / 1.077

Table 4.2: Table listing the investigated petrophysical parameters indicating the mean value, the standard deviation and the minimum and maximum values.

compressional velocity measured in dry and saturated condition (fig. 4.12). In terms of compressional velocity this trend is minor between sample location XF54 and XF57, hence, a distinction is difficult. The electrical resistivity shows a contrary trend as the results decrease from location XF54 to XF57 (fig. 4.12). But also this variation is small and therefore a characterization is uncertain.

The parameters of anisotropy indicate a trend from a prolate shape at sample location XF54 to an oblate shape at location XF57 (fig. 4.8c). The prolate shape may be associated with the ductile deformation of rock material which likely occurred next to the Bavarian Pfahl due to melting processes in the course of the fault forming process. The influence of the melting processes on sample location XF57 is minor and thus the oblate shape impressed is still existent. Furthermore, the degree of anisotropy obtained during the AMS measurement shows a decreasing trend from sample location XF54 to XF57 which confirms the influence of the Bavarian Pfahl on location XF54 (fig. 4.13b).

The measurements in axial and radial direction for the electrical resistivity and the compressional velocity measurements show higher results in axial than in radial direction. In order to characterize the anisotropy structure of the samples two spatial directions (axial, radial) were measured but not the ellipsoidal shape was determined.

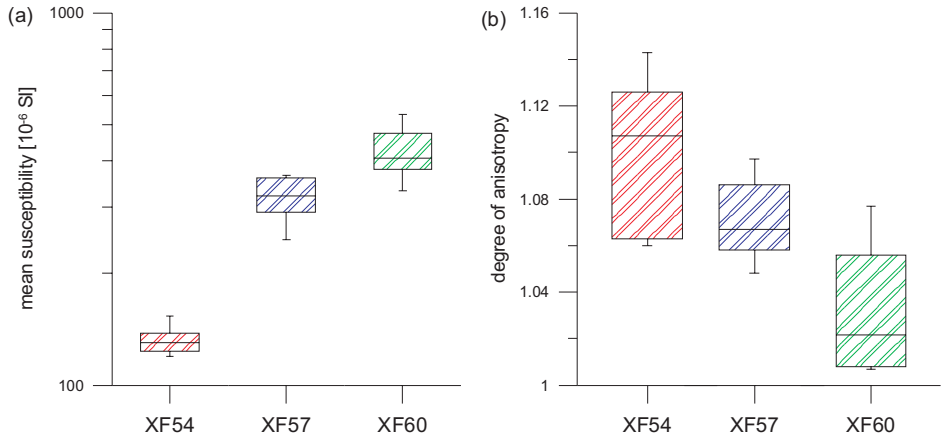

Figure 4.13: (a) Box plot of the mean susceptibility. An increasing trend from sample location XF54 to XF60 is evident. (b) Box plot of the degree of magnetic anisotropy. Sample location XF54 shows the highest anisotropy degree whereas sample location XF60 is indicated by the lowest values.

Hence, the resulting internal structure obtained indicates one preferential direction but can not be interpreted as the real geological structure. However, considering the coefficient of anisotropy a decrease with distance to the Bavarian Pfahl in case of electrical resistivity is evident (fig. 4.6). The ratio calculated for compressional velocity shows almost no variation (fig. 4.10, 4.11).

Comparing sample location XF57 and XF60 all observed parameters show a significant change (fig. 4.12). However, the two sample locations show also affinity as the ratios of mean susceptibility versus NRM plot next to each other and indicate magnetite as magnetization carrier for both locations. A difference is given as the concentration of magnetite at sample location XF57 is slightly lower. This can be seen by the decrease in mean susceptibility from location XF57 to XF60. The comparison of mean susceptibility with degree of magnetic anisotropy indicates related susceptibility values as well as similar degrees of anisotropy. Moreover, the plot of foliation factor versus lineation factor shows an oblate shape for both locations.

Analyzing the porosity value an increase from sample location XF57 to XF60 occurs whereas the bulk density and grain density decreases (fig. 4.12). The decreasing trend is also observed in terms of compressional velocity and electrical resitivity. In order to analyze the anisotropic features of the sample locations the coefficient of anisotropy was calculated. In terms of electrical resisitvity a decrease from sample location XF57 to XF60 exists. The ratio calculated for the compressional velocity shows a small variation. Nevertheless, a decreasing trend is noted.

These results lead to the interpretation that both locations have undergone more or less the same deformation process after the intrusion of the Bohemian Pluton, but have not undergone any ductile deformation processes in course of the fault forming process. The variations in petrophysical parameters between the two locations are caused by the difference in distance to the Bavarian Pfahl and hence, a decreasing influence results.

Summarizing the discussed results the assumption that the influence of the Bavarian Pfahl on the sample locations decreases with increasing distance to the fault is proved. The significant change in the concentration of the magnetization carrier magnetite from sample location XF54 to XF60, evident in the mean susceptibility data and the AF–demagnetization curves, is caused by melting processes due to the formation of the fault system. This change is also evident by the modification of the ellipsoidal shape from prolate shape at sample location XF54 to oblate shape at sample location XF57 and XF60. Furthermore, the degree of magnetic anisotropy as well as the coefficient of anisotropy in terms of electrical resistivity and compressional velocity decreases with increasing distance to the Bavarian Pfahl.

Chapter 5

Bosumtwi Meteorite Impact Crater

5.1 Geology

Ghana, a state within West Africa, hosts one of the youngest meteorite impact crater known on earth (Köberl et. al., 1998)(fig. 5.1). A major part of Ghana is occupied by the Precambrian West African Craton (Pesonen et. al., 2003). Geologically Ghana is subdivided into three different major units: Paleoproterozoic rocks in southwestern and northwestern Ghana, gneisses and supracrustal rocks of mostly Neoproterozoic age in the southeast and east of Ghana and finally flat–lying shelf/marine sediments of very late Precambrian to Paleozoic age in central and northeastern Ghana. Along the coast small strips of mostly Cenozoic sediments are evident (Schlüter, 2006). The basement of Ghana is subdivided into the Birrimian and Tarkwaian Supergroups (Pesonen et. al., 2003).

The Birrimian Supergroup of Paleoproterozoic strata is subdivided into a sedimentary succession consisting of phyllites, tuffs and greywackes overlain by conglomerates, sandstones and shales and a volcanic succession of tholeiitic affinity. In former times the Birrimian Supergroup was subdivided into the Lower Birrimian, dominated by metasediments, and the Upper Birrimian, dominated by greenstone–type metavolcanics. The age of the groups is around 2.17 $\pm$0.07 Ga and therefore a contemporary deposition occurred. Nowadays the lithologies are characterized by the volcanoclastic assemblage emplaced as series of five evenly spaced volcanic belts of almost NE–SW direction (Kibi–Winiba Belt, Ashanti Belt, Asankrangwa Belt, Sefwi Belt, Bole–Navrongo Belt and Lawra Belt), several kilometers long and of low–grade metamorphic tholeiitic lava (Schlüter, 2006). The boundaries are characterized by basins containing dacitic volcaniclastics, wackes, argillitic sediments and granitoids (Köberl et. al.,

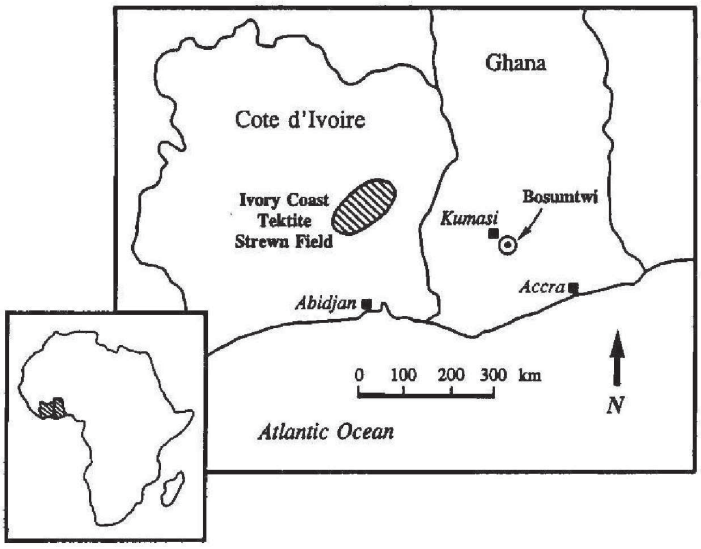

Figure 5.1: Location of the Bosumtwi meteorite impact crater in the Ashanti Province of Ghana/West Africa about 30km southeast of the city of Kumasi (Köberl et. al., 1998).

1998).

The Bosumtwi meteorite impact crater formed around 1.07 Ma ago is located in the Ashanti Province (fig. 5.1). The crater has a rim-to-rim diameter of 10.5km and is almost completely filled by Lake Bosumtwi. The crater rim rises about 250–300m above the lake level.

The formation of an impact crater depends mainly on the size and velocity of the cosmic projectile. In order to create a large impact structure, as the Bosumtwi impact structure, the projectile size has to be 20m in case of coherent iron and 50m in case of a stony object. An extraterrestrial object that strikes the earth surface at its original cosmic velocity produces intense shock waves which radiate outward through the target rock from the point of impact. Due to the high velocity of the cosmic projectile and the resulting shock wave intension the projectile melts and vaporizes almost completely. During the formation process of an impact structure three major stages different in forces and mechanisms occur: contact and compression, excavation and modification. These processes lead to the creation of a simple (bowl-shaped) or complex impact structure (French, 1998).

The contact and compression stage depends not only on the type of cosmic projectile but also on the target rock. Thus, in solid rocks the projectile is stopped immediately and the depth of penetration is no more than 1-2x its own diameter. The resulting shock waves penetrate through the target rock and create the so called shock zones

which are roughly hemispherical. The excavation stage is characterized by the actual open up of the impact crater which is accompanied by complex interactions between the expanding shock waves and the original ground surface. The occurring forces drive the target rock outward from the impact point, producing a symmetric excavation flow which leads to the formation of a bowl-shaped depression, the so called transient crater. After the excavation stage follows the modification where the expanding shock waves have decayed to low-pressure elastic stress waves beyond the crater rim and from this point on gravity and rock mechanic influences modify the transient crater to its impact-related changes (French, 1998).

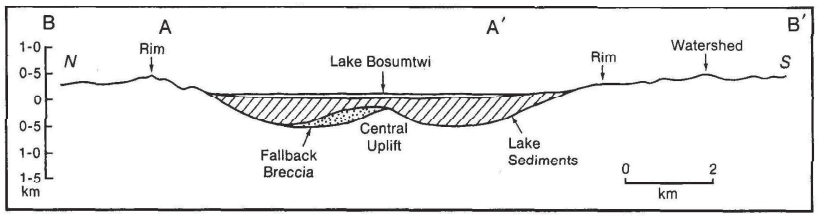

Figure 5.2: Hypothetical north-south cross section of the Bosumtwi impact structure indicating the complex structure with a central uplift, a generally flat floor and an extensive inward collapse, after Jones et. al. (1981) (Köberl et. al., 1998). The drill core LB-07A is located next to the central uplift in the deep crater moat whereas drill core LB-08A is located on the central uplift.

In case of the Bosumtwi meteorite impact structure a complex crater is evident (fig. 5.2). This structure is characterized by a centrally uplifted region, a generally flat floor and extensive inward collapse around the rim (French, 1998). The meteorite impact occurred in lower greenschist facies metasediments of the Birrimian Supergroup (2.1–2.2 Ga) (fig. 5.3). The regional geology around the impact crater is dominated by greywackes and sandstone/quartzitic rocks (fig. 5.3). In the northeastern and southern sectors shale and minor mica schist are present. Furthermore, several Proterozoic granitic intrusions occur as well as a small number of strongly weathered granitic dikes in the crater rim (Köberl et. al., 1998) (fig. 5.3).

The drilling project carried out in the course of the International Scientific Drilling Project (ICDP) in 2004 sinked two deep drill cores into Lake Bosumtwi (fig. 5.4). The core LB-07A was drilled into the deep crater moat about 0.5km north-west of the central uplift to a depth of 545m. The hard rock strata starts at a depth of 338m and therefore a total core length of 207m was available for investigations on consolidated rocks. The core LB-08A was drilled into the outer flank of the central uplift to a depth

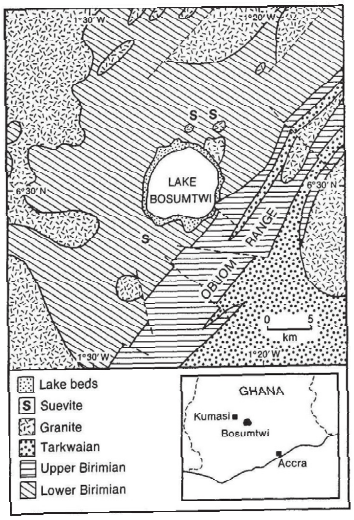

Figure 5.3: Schematic geological map of the Bosumtwi impact structure and surroundings, after Jones et. al. (1981). The division of Upper and Lower Birrimian Supergroup represents a differentiation of rock types as metamorphosed volcanic rocks occur within the Upper Birrimian and metasediments in the Lower Birimian (Köberl et. al., 1998).

of 452m. A total core length of 217m was examined as the bedrock starts at a depth of 235m. The lithologies available in the two drill cores are a polymict lithic breccia, a monomict lithic breccia, suevite, greywacke and a group consisting of shale, slate, schist and phyllite (in the following referred to as shale group).

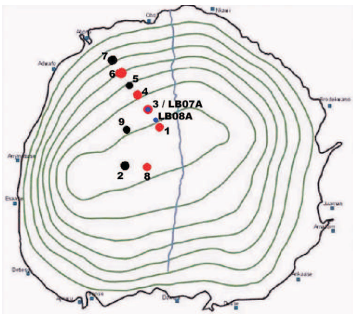

Figure 5.4: Locations of drill sites superimposed on lake bathymetry. The drilled sediment holes are red, the impact rock holes are blue (Conze, 2006, ICDP Homepage, Bosumtwi Project).

5.2 Results

In January 2005 the selection of the samples was carried out in the GeoForschungsZentrum Potsdam, Germany. At the Petrophysics Laboratory of the University of Leoben,

cylindrical shaped plugs with a diameter of 19mm and a length of 22mm were drilled out of the source rock. Due to fragile source rocks the preparation of plugs was not always possible and therefore only a total amount of 16 samples were examined.

LB-07A			LB-08A		
lithology	**depth [m]**	**total number of samples**	**lithology**	**depth [m]**	**total number of samples**
polymict lithic breccia	346.96 – 347.19	2	polymict lithic breccia	236.03 – 238.95	6
shale group	349.26	4	suevite	239.36	2
polymict lithic breccia	349.50	1	polymict lithic breccia	241.70	1
suevite	354.20 – 368.90	8	suevite	255.45 – 258.74	12
polymict lithic breccia	371.42	1	greywacke	271.41 – 283.20	14
shale group	375.04	4	shale group	285.32	2
polymict lithic breccia	376.00	4	greywacke	297.39 – 350.63	11
suevite	380.76 – 385.41	12	shale group	355.12	2
polymict lithic breccia	389.36 – 404.45	18	greywacke	356.97 – 435.39	18
suevite	408.09 – 409.97	5			
	Σ	59		Σ	68

Figure 5.5: Listing of the lithologies observed within the drill cores LB–07A and LB–08A, depth indication and total number of samples investigated.

Bulk density and porosity were obtained as standard petrophysical parameters. Unfortunately electrical and elastic properties could not be measured due to the fragile condition of the plugs and their dissolution during the saturation process. The magnetic properties were examined using the Kappabridge KLY-2 (Geofyzika Brno) and the 2G DC–SQUID magnetometer.

In the course of the ICDP–Project a cooperation of three working groups (Division of Geophysics, Department of Physical Sciences, University of Helsinki, Finland; Geologisch-Paläontologisches Institut, Ruprecht-Karls-Universität Heidelberg, Germany; Chair of Geophysics, Department of Applied Geosciences and Geophysics, University of Leoben, Austria) was established. As the three parties used the same methods of measurement but different features of the magnetic properties were examined, the exchange of data enlarged the possibilities of investigations of each group. Therefore a total amount of 127 sample measurements and results are used within this survey. An overview on the lithologies, the depth levels and the respective amount of samples as well as the total amount of samples is listed in fig. 5.5.

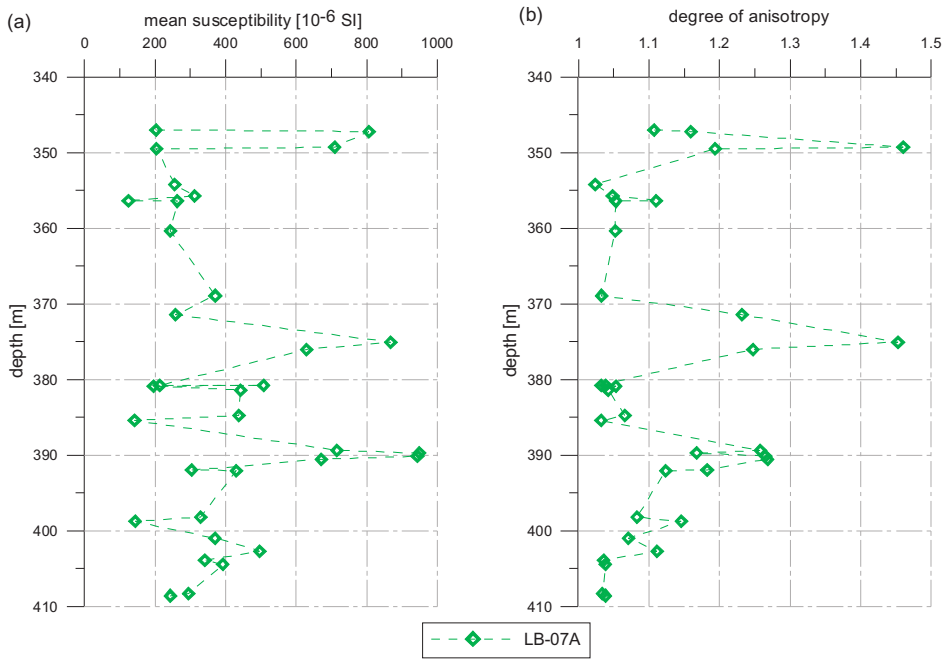

Figure 5.6: (a) Plot of mean susceptibility values [$10^{-6}SI$] versus depth [m]. A baseline of susceptibility is evident at 250·$10^{-6}SI$, outliers occur at depth levels of 350m, 375m and around 390m; (b) Plot of the anisotropy degree versus depth [m]. Peaks in the anisotropy degree occur at depth levels of 350m, 375m and around 390m.

5.2.1 Drill core LB-07A

In drill core LB-07A three lithologies have to be distinguished: the polymict lithic breccia, the suevite and the shale group. The other lithologies available in the drill core are not sampled within this survey.

The mean susceptibility varies in a range from 125 to 867·$10^{-6}SI$ (fig. 5.6a). Although the values vary from one depth level to another a baseline of susceptibility around 250·$10^{-6}SI$ is evident. At the depth levels of 350m, 375m and around 390m peaks of the susceptibility values are observed. The degree of anisotropy varies in a range of 1.024 to 1.460 which indicates a fluctuation from a low degree of anisotropy of 2% to a high anisotropy degree of 46%. The course of the graph shows that the most frequent degree of anisotropy is around 5%. The high values of the anisotropy degree peak out at depth levels of 350m, 375m and around 390m (fig. 5.6b).

Plotting the degree of anisotropy versus the mean susceptibility a trend can be observed that a low degree of anisotropy correlates with a low value of mean susceptibility (fig. 5.7a). Hence, a positive increase towards higher values in both the degree of anisotropy and the mean susceptibility can be seen. Considering the parameters sep-

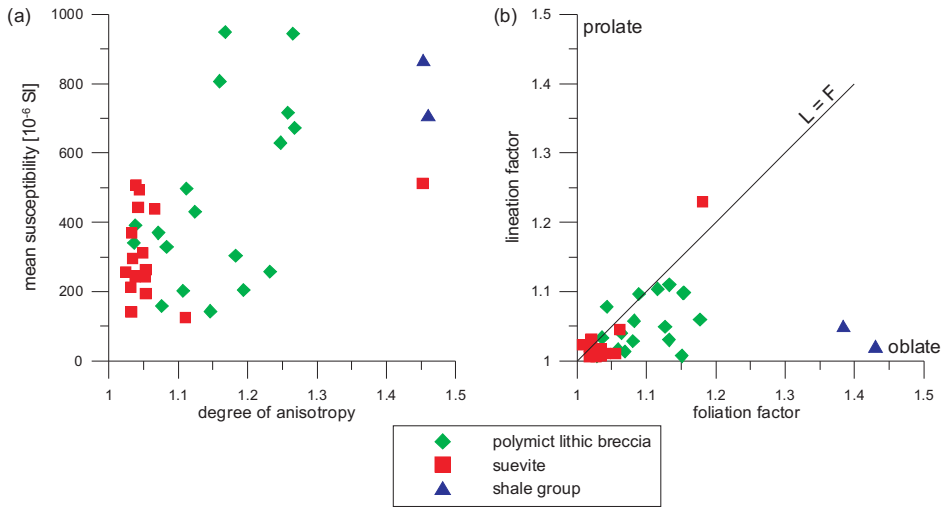

Figure 5.7: (a) Plot of mean susceptibility values [$10^{-6}SI$] versus degree of anisotropy indicating a positive correlation. The mean susceptibility values increases with increasing degree of anisotropy; (b) Cross plot of foliation factor versus lineation factor shows a predominant oblate shape. The solid line acts as borderline between oblate and prolate shape as well as indication for the triaxial shape.

arately for each lithology the polymict lithic breccia varies in a broad range in degree of anisotropy as well as in mean susceptibility. The suevite shows a grouping around a value of 1.050 for the anisotropy degree and an average susceptibility of $300{\cdot}10^{-6}SI$ with one outlier towards higher values in terms of anisotropy degree. The shale group is indicated by a value for mean susceptibility around $800{\cdot}10^{-6}SI$ and the degree of anisotropy plots around 1.450.

The analysis of the shape of the anisotropy ellipsoid plotting the lineation factor versus foliation factor displays a predominant oblate shape for all lithologies observed (fig. 5.7b). The solid line in the plot indicates the borderline between oblate and prolate shape as well as the triaxial shape. The shale group shows the highest values in the degree of anisotropy and the foliation factor which results in a significant oblate shape. The polymict lithic breccia follows next indicated by a lower anisotropy degree and foliation factor, but the overall shape is oblate. The suevite has the lowest anisotropy degree and the cross plot of foliation to lineation factor results in an almost triaxial shape.

In fig. 5.1 a summary of all results obtained for core LB-07A is plotted indicating the mean value, the respective standard deviation and the minimum and maximum value.

LB-07A	polymict lithic breccia			suevite			shale group		
	mean value	std deviation	min/max	mean value	std deviation	min/max	mean value	std deviation	min/max
mean susceptibility [10-6 SI]	463,890	254,530	143.40 / 949.16	315,950	124,990	125.00 / 511.53	788,590	79,590	709.00 / 868.17
lineation factor	1,053	0,035	1.007 / 1.110	1,030	0,052	1.006 / 1.229	1,036	0,015	1.021 / 1.050
foliation factor	1,095	0,048	1.019 / 1.177	1,039	0,039	1.017 / 1.181	1,407	0,023	1.384 / 1.431
degree of anisotropy	1,15	0,076	1.036 / 1.268	1,072	0,10	1.024 / 1.452	1,46	0,00	1.453 / 1.460

Table 5.1: Table reporting the results obtained measuring the mean susceptibility, the degree of anisotropy and the lineation and foliation factor on samples of the LB-07A core. The table includes the mean values, the respective standard deviation and the minimum and maximum values.

5.2.2 Drill core LB-08A

Within the drill core LB-08A, polymict lithic breccia, suevite, greywacke and the shale group are evident and covered in this study. The mean susceptibility of the LB-08A drill core varies in a range of 91 to $572{\cdot}10^{-6}SI$ (fig. 5.8a). The course of the graph is discontinuous but at the susceptibility value of $200{\cdot}10^{-6}SI$ a baseline is present. Referring to the baseline two peaks are significant at depth levels of 280m and 350m. The degree of anisotropy of the LB-08A drill core varies in the range of 1.033 to 1.643 (fig. 5.8b). The highest degree of anisotropy is 64% whereas the most frequent degree of anisotropy is found around 20%. The highest values of anisotropy are found at depth levels of 285m and 355m.

Observing the degree of anisotropy plotted versus the mean susceptibility the shale group is indicated by the highest anisotropy degree around 1.500 and mean susceptibility values of 179.00 and $571.20{\cdot}10^{-6}SI$. The polymict lithic breccia spreads out over a range of 250 to $350{\cdot}10^{-6}SI$ for the mean susceptibility and for the anisotropy degree a variation between 1.100 and 1.250 is observed. In case of suevite the mean susceptibility varies in the range of 50 to $400{\cdot}10^{-6}SI$. The degree of anisotropy plots around 1.050. The mean susceptibility of the greywacke varies between 100 and $550{\cdot}10^{-6}SI$. The degree of anisotropy shows a variation between 1.050 and 1.400.

The shape of the anisotropy ellipsoid varies within this drill core although the overall trend points towards an oblate shape. The polymict lithic breccia, the suevite as well as the shale group are indicated by an oblate shape (fig. 5.9b). The results obtained for the greywacke spread out around the triaxial boundary tending to an oblate shape. The shale group indicated by the highest anisotropy degree shows a significant oblate

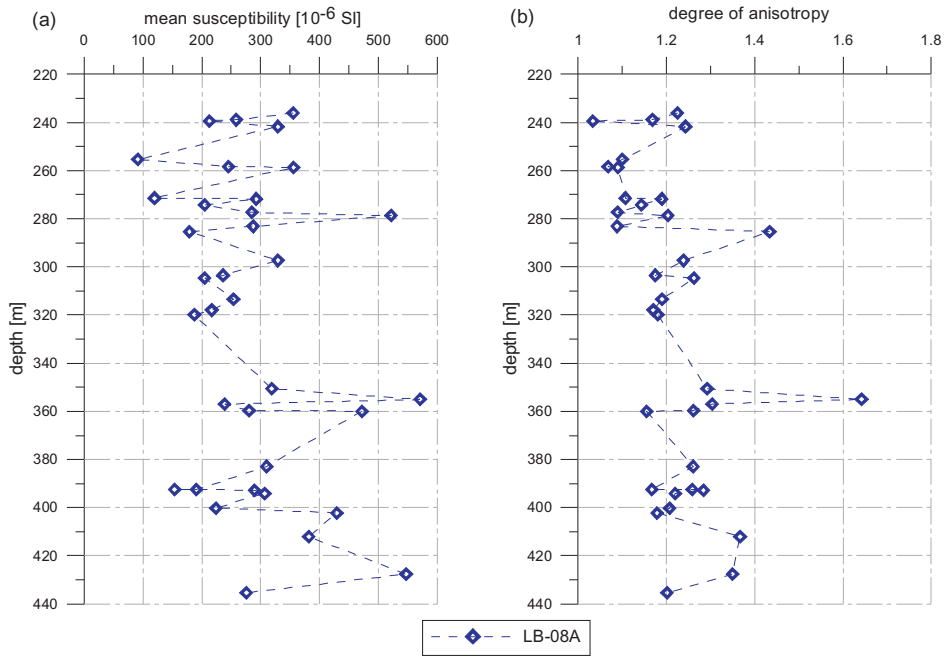

Figure 5.8: (a) Plot of mean susceptibility values [$10^{-6}SI$] versus depth [m]. A baseline of susceptibility is evident at 200·$10^{-6}SI$, outliers occur at depth levels of 280m and 350m; (b) Plot of the anisotropy degree versus depth [m]. Peaks in the anisotropy degree occur at depth levels of 280m and 350m.

shape. The polymict lithic breccia shows the same anisotropy degree as well as oblate shape as the greywacke. The suevite is indicated by the lowest value of anisotropy degree and a faintly pronounced oblate shape.

Tab. 5.2 indicates the results for all investigated parameters for core LB-08A listing the mean values, the respective standard deviation and the minimum and maximum value.

5.3 Discussion

In case of Bosumtwi the meteorite impact is the looming event for the magnetic fabric and structure. As the single lithologies react different to the impact event the magnetic fabrics evident in the samples can be seen as distinguishing criterion for the lithologies involved. Previous studies on this issue performed by e.g. Tarling & Hrouda (1993) and Chadima et al. (2006) state that the influence of destructive events persistently changes the magnetic fabric and thus gives an opportunity to differentiate among various lithologies. Analyzing the data of the parameters presented in the results section

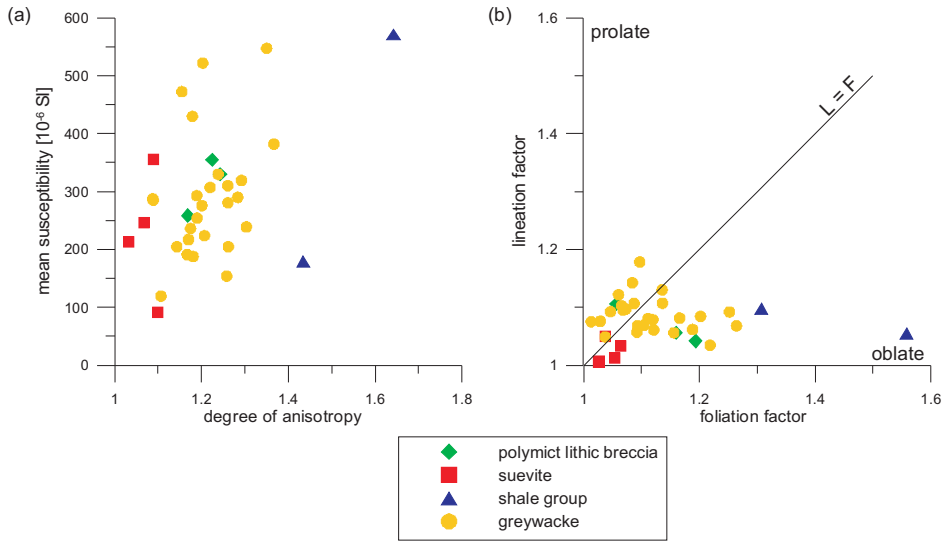

Figure 5.9: (a) Plot of mean susceptibility values $[10^{-6}SI]$ versus degree of anisotropy. A variation in results is given in both parameters, mean susceptibility and degree of anisotropy, for all investigated lithologies; (b) Cross plot of foliation factor versus lineation factor shows a predominant oblate shape for the lithologies of polymict lithic breccia, suevite, shale group and greywacke. The solid line is the indicator for the triaxial shape and acts as boundary between prolate and oblate shape.

LB-08A	polymict lithic breccia			suevite			shale group			greywacke		
	mean value	std deviation	min/max	mean value	std deviation	min/max	mean value	std deviation	min/max	mean value	std deviation	min/max
mean susceptibility [10-6 SI]	314,490	40,880	258.60 / 355.23	226,450	94,490	91.00 / 356.17	375,100	196,100	179.00 / 571.20	290,750	104,440	119.33 / 547.20
lineation factor	1,068	0,028	1.168 / 1.243	1,026	0,017	1.006 / 1.050	1,076	0,021	1.054 / 1.097	1,087	0,031	1.035 / 1.178
foliation factor	1,136	0,058	1.042 / 1.106	1,045	0,014	1.027 / 1.064	1,433	0,125	1.307 / 1.558	1,116	0,065	1.013 / 1.264
degree of anisotropy	1,21	0,032	1.056 / 1.193	1,073	0,03	1.033 / 1.099	1,54	0,10	1.434 / 1.643	1,21	0,07	1.088 / 1.367

Table 5.2: Table reporting the results obtained measuring the mean susceptibility, the degree of anisotropy and the lineation and foliation factor on samples of the LB-08A core. The table includes the mean values, the respective standard deviation and the minimum and maximum values.

distinguishable features in terms of degree of anisotropy and lineation and foliation factor are evident.

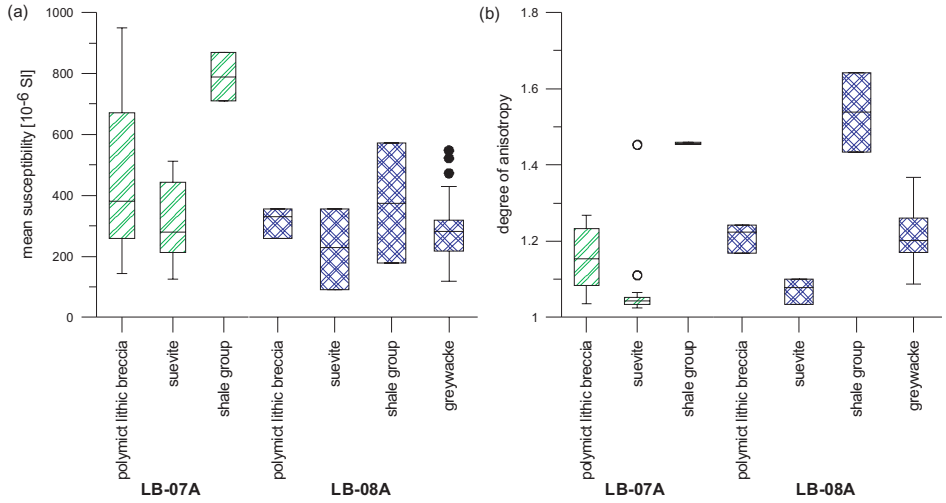

Figure 5.10: (a) Box plot of mean susceptibility values [$10^{-6}SI$]. The results plot within the same range and hence, a differentiation is uncertain; (b) Box plot of the anisotropy degree indicating slightly higher values in case of LB-08A.

The mean susceptibility values for drill core LB-07A and LB-08A plot within the same range (fig. 5.10a). However, the degree of anisotropy shows a variation between the two drill cores (fig. 5.10b) as core LB-08A has a slightly higher anisotropy degree than core LB-07A. The rocks in the central uplift as sampled in the LB-08A core were located in larger depths before the impact event occurred. The central uplift is characterized to consist of deeper rocks lifted after the meteorite impact (French, 1998). Hence, the rocks do already have a higher degree of anisotropy due to greater burial depth than the rocks in the present surrounding area.

In fig. 5.11, foliation and lineation factors of the two drill cores are compared. The results plot within the same range with slightly higher values for core LB-08A. In terms of foliation factor the high values for the shale group are eye-catching. Comparing the factors with each other, the foliation factor tends to higher values than the lineation factor (fig. 5.11) which indicates the oblate shape.

In terms of mean susceptibility the values allow no distinction between the two cores whereas a comparison versus depth shows significant changes with respect to lithology (fig. 5.12). In order to characterize the LB-07A core for the polymict lithic breccia mean susceptibility values around $464{\cdot}10^{-6}SI$. With results for the mean susceptibility around $316{\cdot}10^{-6}SI$ for the suevite a distinction is observed. Two peaks at depth levels of 350m and 360m ($789{\cdot}10^{-6}SI$) are correlated with small shale group layers.

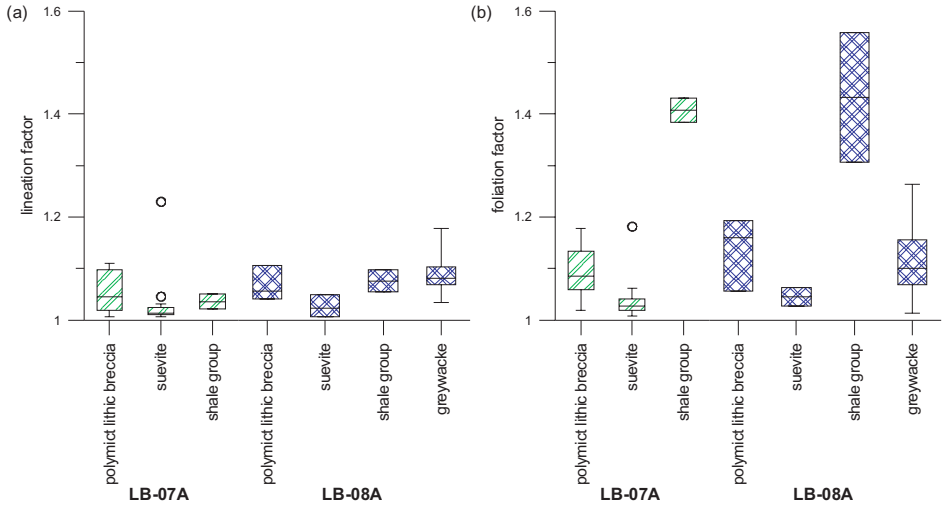

Figure 5.11: (a) Box plot of the lineation factor indicating slightly lower values for LB-07A although in comparison to the foliation factor the results are significant lower; (b) Box plot of the foliation factor. The lithologies available in LB-07A have lower values than the rock types in LB-08A. In comparison to the lineation factor the foliation factor is higher indicating an oblate shape.

Considering the results of the degree of anisotropy and plotting them versus depth peaks as stated in terms of mean susceptibility occur (fig. 5.12). The shale group responsible for the peaks has an anisotropy degree around 1.460. The polymict lithic breccia is characterized by an anisotropy degree around 1.150 whereas suevite has a degree of anisotropy of 1.070. This allows a differentiation of the three lithologies.

In case of the LB-08A core the characterization of layer boundaries is difficult as the lithologies change rapidly in very small ranges of about 0.5m as determined by the Bosumtwi working group and therefore not all layers are included within the sampling interval. Hence, a detailed indication of layer boundaries is uncertain. Regarding this problem only a coarse division between the observed lithologies is possible and insertions of other lithologies are assumed. The course of the anisotropy degree with a layer indication is plotted in fig. 5.13. In the depth range of 230m and 245m a layer of polymict lithic breccia is observed. An interruption occurs at 240m with a lower degree of anisotropy and mean susceptibility which is identified as suevite. This layer is a first indicator for the rapid changes in lithology within the drill core which are sampled by accident. Following the polymict lithic breccia a layer of suevite is observed indicated by similar values obtained for the first suevite insertion. Starting at a depth of 260m greywacke is the predominant lithology observed. Interruptions of the greywacke by layers of the shale group are observed at depth levels of 285m and 355m. The shale

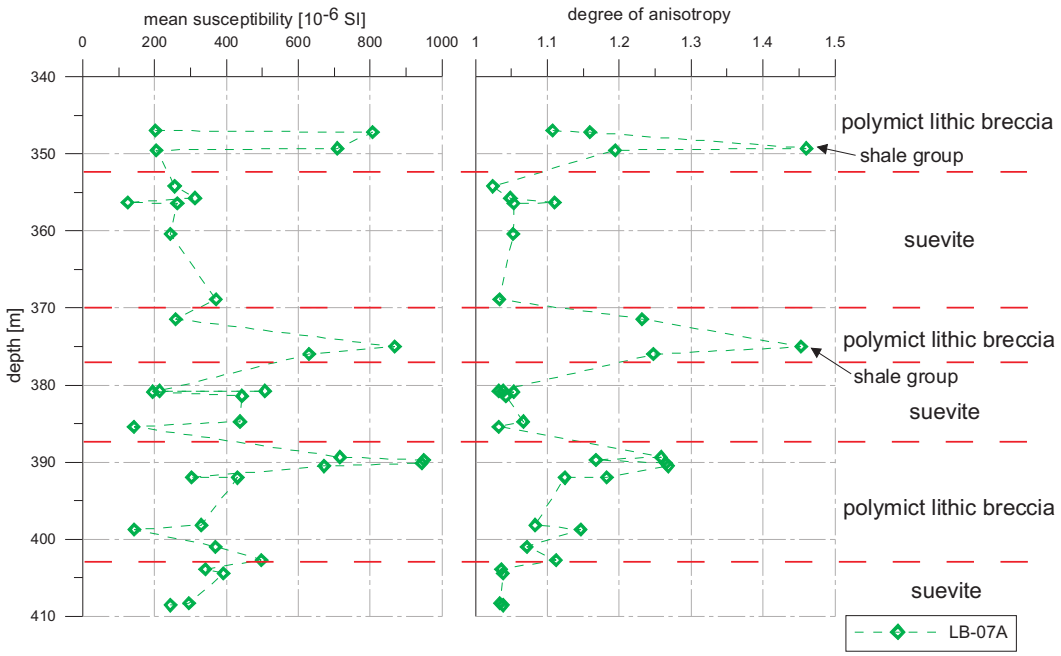

Figure 5.12: Plot of mean susceptibility values [$10^{-6}SI$] and the degree of anisotropy versus depth [m]. The horizontal dashed lines indicate the layer boundaries. A simplified description of the lithology sequence of the LB-07A core is plotted next to the diagram.

group layers show significant higher values in both degree of anisotropy and mean susceptibility. The results for the anisotropy degree allow a distinction of the various layers involved. Considering the results of the mean susceptibility measurement solely the definition of the layers is uncertain, but combined with the results of the anisotropy degree measurement a support is obtained.

In conclusion it can be stated that the mean susceptibility values are undistinguished between the two drill cores LB-07A and LB-08A, but considering the changes in susceptibility with increasing depth within the cores a distinction between the layers is possible. Considering the degree of anisotropy the two boreholes can be differentiated as LB-07A shows a lower anisotropy degree than LB-08A. Furthermore, an analysis of the two drill cores in terms of the anisotropy degree allows us to define layer boundaries. A restriction has to be set if the layer thickness changes in intervals smaller than 0.5m as this variation is too rapid for a resolution with the sample interval of this study. The investigation of the anisotropy ellipsoid yields to a further characterization of the single lithologies. Distinguishing criterions for the lithologies can be defined and these criterions are helpful in setting the layer boundaries.

Summarizing the present study it can be stated that petrophysical parameters allow a differentiation of various lithologies. The analysis in view of the anisotropy of

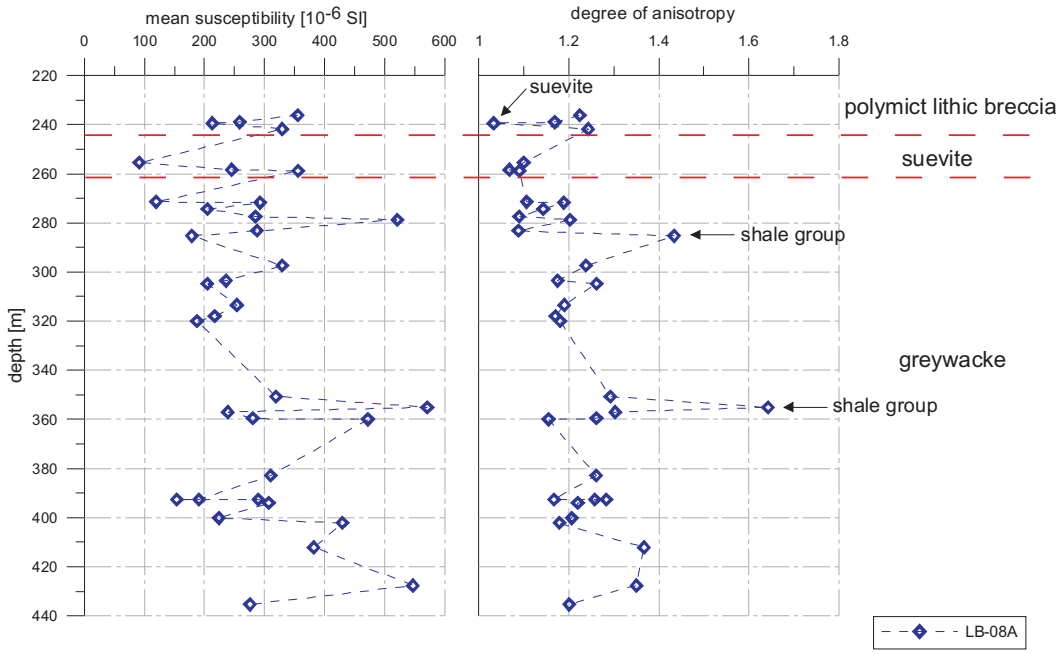

Figure 5.13: Plot of mean susceptibility values [$10^{-6}SI$] and the degree of anisotropy versus depth [m]. The horizontal dashed lines indicate the layer boundaries. A simplified description of the lithology sequence of the LB-08A core is plotted next to the diagram.

petrophysical parameters offers a further characterization of the involved lithologies.

Chapter 6

Conclusion

The study at hand investigated three locations in terms of their petrophysical properties and directional dependence in order to determine a characterization of the lithologies involved and the internal structure.

The analysis of the petrophysical parameters of the shield volcano of Bad Gleichenberg yielded to a differentiation of various lithologies. The affinity of some lithologies allowed the identification of weathering zones caused by hydrothermal fluids. The investigation by means of the anisotropy coefficient was uncertain as the values plot randomly and unoriented which is correlated to the fact that the shield volcano was not involved in a destructive event after its formation process.

The investigation within the Bohemian Massif of Austria showed a dependence of petrophysical properties of Schlägel granite with varying distance to the Bavarian Pfahl. The analysis of the measurements showed mineralogical variations as well as structural deformations and thus, a correlation between distance and influence of the Bavarian Pfahl on the sample sites was observed. The fault forming process was accompanied by high temperatures and ductile deformation processes which are likely responsible for these variations.

The meteorite impact crater of Bosumtwi, Ghana, was observed by means of two drill cores. The susceptibility measurements allowed no differentiation between the two cores. However, investigating each core a characterization of the lithologies involved was possible. The analysis of the anisotropy degree lead to further information and thus, a core description indicating the lithologies and their boundaries was obtained.

In conclusion it can be stated that the investigation of petrophysical parameters and the degree of anisotropy allows a characterization of geological structures and the lithologies involved.

Chapter 7

Bibliography

Belocky R., Seiberl W. and Slapansky P. 1996. *Verifizierung und fachliche Bewertung von Forschungsergebnissen und Anomaliehinweisen aus regionalen und überregionalen Basisaufnahmen und Detailprojekten.* ÜLG–28/95, Wien: Geologische Bundesanstalt, Fachabteilung Geophysik. 96pp.

Carmichael, *R.S.* 1989. *Practical Handbook of Physical Properties of Rocks and Minerals.* CRC Press, Boca Raton Florida. 755pp.

Chadima *M.,* Hrouda *F.* and Melichar *R.* 2006. *Magnetic fabric study of the SE Rhenohercynian Zone (Bohemian Massif): Implications for dynamics of the Paleozoic accretionary wedge.* Tectonophysics 418:93–109.

Conze *R.* 2006. *Lake Bosumtwi Drilling project.* source accessed August/September 2006. http://www.icdp-online.de/contenido/icdp/front_content.php?idcat=391.

Crampin *S.* and Lovell *J.H.* 1991. *A decade of shear-wave splitting in the Earths crust: what does it mean? what use can we make of it? and what should we do next?.* Cited in: Schön, J.H., 2004. Physical Properties of Rocks: Fundamentals and Principles of Petrophysics, Chapter 6, pp. 133–282, Handbook of Geophysical Exploration, Seismic Exploration, Volume 18, Elsevier.

Ebner *F.* 1981. *Vulkanische Tuffe im Miozän der Steiermark.* Mitteilung des naturwissenschaftlichen Vereins Steiermark 111:39–55.

Ebner *F.* 1990. *Rohstoffpotential des Steirischen Tertiärbeckens.* Berg- und Httenmnnische Monatshefte 135:363–371.

Ebner *F.* 1992. *Vulkanismus im steirischen Becken.* Mitteilung der Österreichischen Mineralogischen Gesellschaft 137:231–242.

Ebner *F.* 1997. *Die geologischen Einheiten Österreichs und ihre Rohstoffe.* Cited in: Archiv für Lagerstätten Forschung, Band 19, edited by Weber L. Wien: Geologische Bundesanstalt. pp. 49–229.

EBNER *F.* AND SACHSENHOFER *R.F.* 1991. *Die Entwicklungsgeschichte des Steirischen Tertiärbecken.* Heft 49. Graz: Mitteilungen der Abteilung für Geologie und Paläontologie am Landesmuseum Joanneum. 82pp.

FRANK *W.,* SCHARBERT *S.,* THÖNI *M.,* POPP *F.* AND HAMMER *S.* 1990. *Isotopengeologische Neuergebnisse zur Entwicklungsgeschichte der Böhmischen Masse.* Projekt S 47-GEO, Österreichische Beiträge zu Meterologie und Geophysik 3:185–228.

FRENCH *B.M.* 1998. *Trace of catastrophe.* Houston: LPI Contribution No. 954, Lunar and Planetary Institute 120pp.

FRIEDL *G.,* FINGER *F.,* PAQUETTE *J.-L.,* VAN QUADT *A.,* MCNAUGHTON *N.J.* AND FLETCHER *I.R.* 2004. *Pre-Variscian geological events in the Austrian part of the Bohemian Massif deduced from U-Pb zircon ages.* International Journal of Earth Science 93:802–823.

FRITZ*, I.* 2002. *Schlacken–Tuffe–Maare, Eine Studienreise zu den Vulkanruinen der Oststeiermark.* Exkursionsführer, 22.–23.05.2002.

GEOLOGISCHE BUNDESANSTALT 2006. *Geowissenschaftliche Übersichtskarten.* source accessed September/October 2006. http://www.geologie.ac.at/.

HOUSEN *B.A.,* AND KANAMATSU *T.* 2003. *Magnetic fabric from the Costa Rica margin: sediment deformation during the initial dewatering and underplating process.* Earth and Planetary Science Letters 206:215–228.

JÄGER *A.* 2004. *Vulkanite der Oststeiermark.* BerichtVALL-Projekt. 42pp.

KELLER*, G.V. and* FRISCHKNECHT*, F.C.* 1966. *Electrical methods in geophysical prospecting.* Cited in: Schön, J.H., 2004. Physical Properties of Rocks: Fundamentals and Principles of Petrophysics, Chapter 9, pp. 379–478, Handbook of Geophysical Exploration, Seismic Exploration, Volume 18, Elsevier.

KÖBERL*, C.,* REIMOLD*, W.U.,* BLUM*, J.D.,* AND CHAMBERLAIN*, C.P.* 1998. *Petrology and geochemistry of target rocks from the Bosumtwi impact structure, Ghana, and comparison with Ivory Coast tektites.* Geochimica et Cosmochimica Acta 62:2179–2196.

KRENMAYR*, H.G.,* HOFMANN*, T.,* MANDL*, G.W.,* PERESSON*, H.,* PESTAL*, G.,* PISTOTNIK*, J.,* REITNER*, J.,* SCHARBERT*, S.,* SCHNABEL*, W.* AND SCHÖNLAUB*, H.P.* 2000. *Rocky Austria, An illustrated Earth History of Austria.* Geological Survey of Austria, Vienna 2000. 60pp.

KUKKONEN*, I.T.,* KIVEKÄS*, L.,* AND PAANANEN*, M.* 2003. *Physical Properties of (impact melt), suevite and impact breccia in the Lappajärvi meteorite crater, Finland.* Tectonophysics 216:111–122.

Lenz, *B.,* Mauritsch, *H.J.,* and Reisinger, *J.R.* 1996. *Petrophysical investigations in the Southern Bohemian Massif (Austria): data–aquisition, -organisation and -interpretation.* Mineralogy and Petrology 58:279–300.

Mauritsch *H.J.* and Reisinger *J.* 1990. *Paläomagnetische Untersuchungen in der Böhmischen Masse.* Projekt S 47-GEO, Österreichische Beiträge zu Meterologie und Geophysik 3:25–42.

Olhoeft, *G.R.* 1985. *Electrical Properties of Rocks and Minerals.* Cited in: Schön, J.H., 2004. Physical Properties of Rocks: Fundamentals and Principles of Petrophysics, Chapter 9, pp. 379–478, Handbook of Geophysical Exploration, Seismic Exploration, Volume 18, Elsevier.

Olhoeft, *G.R.* and Johnson, *G.R.* 1989. *Densities of Rocks and Minerals.* Cited in: Carmichael, R.S., 1989. Practical Handbook of Physical Properties of Rocks and Minerals, Section II, CRC Press, Boca Raton Florida. 775pp.

Parés, *J.M.* and van der Pluijm, *B.A.* 2002. *Evaluating magnetic lineations (AMS) in deformed rocks.* Tectonophysics 350:283–298.

Pesonen, *L.J.,* Köberl *C.* and Hautaniemi, *H.* 2003. *Airborne Geophysical Survey of the Lake Bosumtwi Meteorite Impact Structure (Southern Ghana) – Geophysical Maps with Descriptions.* Jahrbuch der Geologischen Bundesanstalt 143:581–604.

Scholger, *R.* and Mauritsch, *H.J.* 1992. *Petrophysikalische Untersuchungen an Bohrkernen des nördlichen Wiener Beckens (Autochtones Mesozoikum).* Leobner Hefte zur Angewandte Geophysik 4:88–95.

Schön, *J.H.* 2004. *Physical Properties of Rocks: Fundamentals and Principles of Petrophysics.* Oxford: Elsevier Ltd. 583pp.

Schlüter, *T.* 2006. *Geological Atlas of Afrikca.* Berlin–Heidelberg: Springer–Verlag. 272pp.

Soffel, *H.C.* 1991. *Paläomagnetismus und Archäomagnetismus.* Berlin–Heidelberg: Springer–Verlag. 276pp.

Sruoga *P.,* Rubinstein, *N.* and Hinterwimmer, *G.* 2004. *Porosity and permeability in volcanic rocks: a case study on the Serie Tobífera, South Patagonia, Argentina.* Journal of Volcanology and Geothermal Research 132:31–43.

Tarling *D.H.* and Hrouda *F.* 1993. *The Magnetic Anisotropy of Rocks.* London: Chapman & Hall. 217pp.

Telford *W.M.,* Geldart, *L.P.* and Sheriff, *R.E.* 1990. *Applied Geophysics.* Second Edition, Cambridge University Press, Cambridge. 770pp.

Tollmann *A.* 1985. *Geologie von Österreich, Ausserzentralalpiner Anteil.* Band

II, Franz Deuticke Wien. 710pp.

Wallbrecher *E.,* Brandmayr *M.* and Handler *R.* 1990. *Kinematische Untersuchungen an Blattverschiebungszonen in der südlichen Böhmischen Masse.* Projekt S47-GEO, Österreichische Beiträge zu Meteorologie und Geophysik, Heft 3:97–120.

Wallbrecher *E.,* Brandmayr *M.,* Handler *R.,* Loizenbauer *J.,* Maderbacher *F.* and Platzer *R.* 1993. *Konjugierte Scherzonen in der südlichen Böhmischen Masse: variszische und alpidische kinematische Entwicklungen.* Projekt S4713, Mitteilung der Österreichischen Mineralogischen Gesellschaft 138:237–252.

Zechner *M.* 2002. *Die Anisotropie petrophysikalischer Parameter in Abhängigkeit von Gefüge und Wassersättigung untersucht am Beispiel des Plattengneises.* Diploma thesis, Chair of Geophysics, Department of Applied Geosciences and Geophysics, University of Leoben, Leoben, Austria. 74pp.

Vanorio *T.,* Prasad *M.,* Patella *D.* and Nur *A.* 2002. *Ultrasonic velocity measurements in volcanic rocks: correlation with microtexture.* Geophysical Journal International 149:22–36.

List of Figures

List of Tables